Enhancing Compton Camera Imaging with Neural Networks

J. Pérez-Curbelo, J. Roser, L. Barrientos, R. Viegas, M. Borja-Lloret,

J. V. Casaña, F. Hueso-González, A. Ros, K. Brzezinski, V. Sanz and G. Llosá

Instituto de Física Corpuscular IFIC (CSIC-UV)

http://ific.uv.es/iris

Image **R**econstruction, **I**nstrumentation and **S**imulations in medical applications

Outline

- Introduction to Compton Cameras
- MACACO Compton Camera
- Application of Neural Networks to Enhance MACACO Compton Camera Imaging
  - Event Selection with Multi-Energy Radioactive Sources
  - Photon Interaction Localization in Monolithic Crystals
  - Background Reduction for Proton Range Verification
- Conclusions

Outline

- **Introduction to Compton Cameras**
- MACACO Compton Camera
- Application of Neural Networks to Enhance MACACO Compton Camera Imaging
  - Event Selection with Multi-Energy Radioactive Sources
  - Photon Interaction Localization in Monolithic Crystals
  - Background Reduction for Proton Range Verification
- Conclusions

Compton cameras

- Compton camera: electronically collimated device.
  - Cone surface from measured positions and energies, if E_o is known or can be measured.
  - Cone intersection.

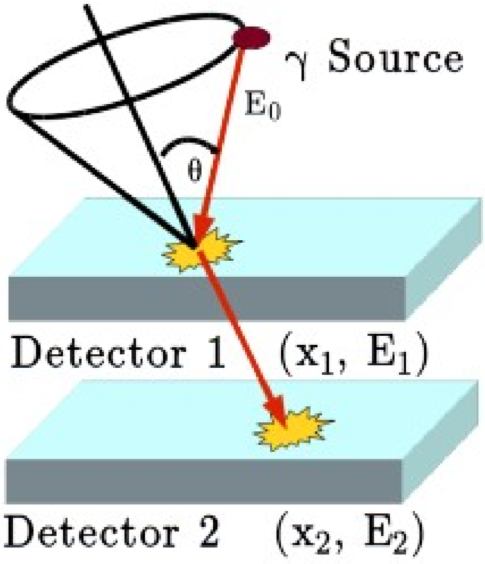

$$cos\theta = 1 - mc^2 \left(\frac{1}{E_0 - \tilde{E}_1} - \frac{1}{E_0} \right)$$

Compton cameras

- Compton camera: electronically collimated device.
  - Cone surface from measured positions and energies, if E_o is known or can be measured.
  - Cone intersection.

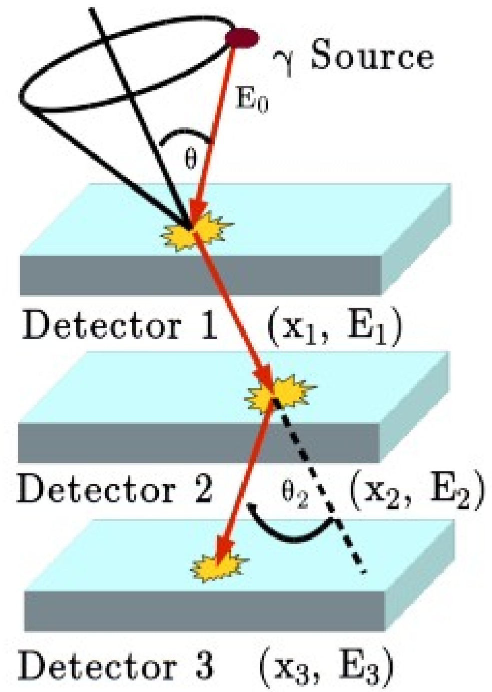

$$cos\theta = 1 - mc^2 \left(\frac{1}{E_0 - \tilde{E}_1} - \frac{1}{E_0} \right)$$

Compton cameras

Physics experiments

V. Schonfelder 1991 Adv. Space Res. 11(8), pp. (8) 313—(8) 322

Location of radioactive sources

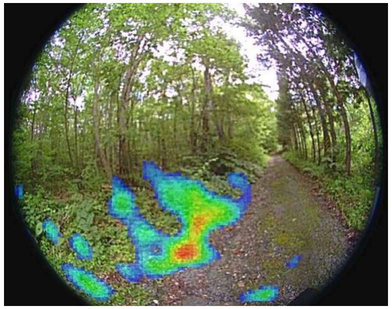

Compton cameras

Physics experiments

V. Schonfelder 1991 Adv. Space Res. 11(8), pp. (8) 313—(8) 322

Location of radioactive sources

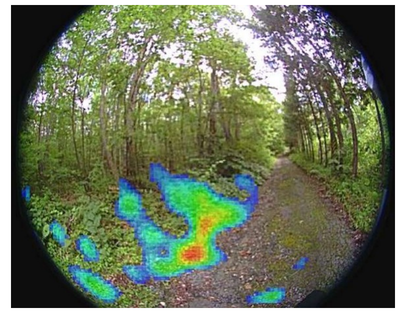

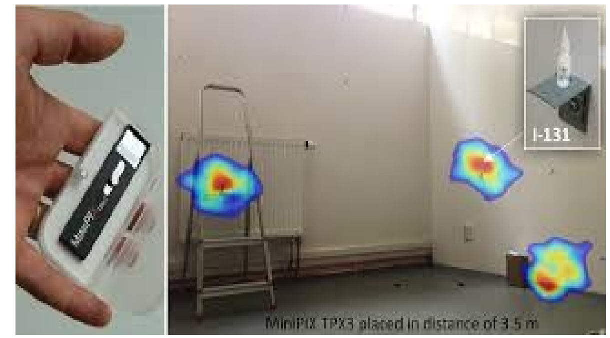

Imaging in nuclear medicine

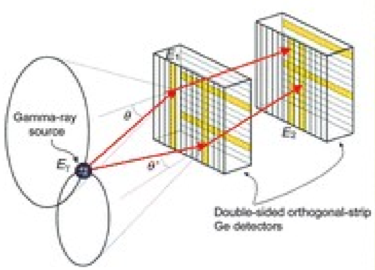

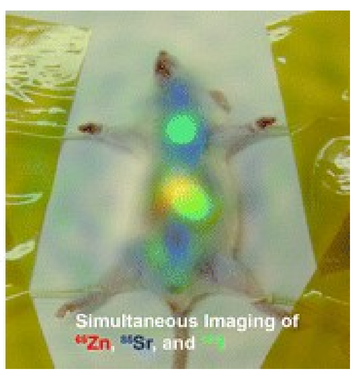

Shinji Motomura et al 2008 J. Anal. At. Spectrom. 23, 1089-1092

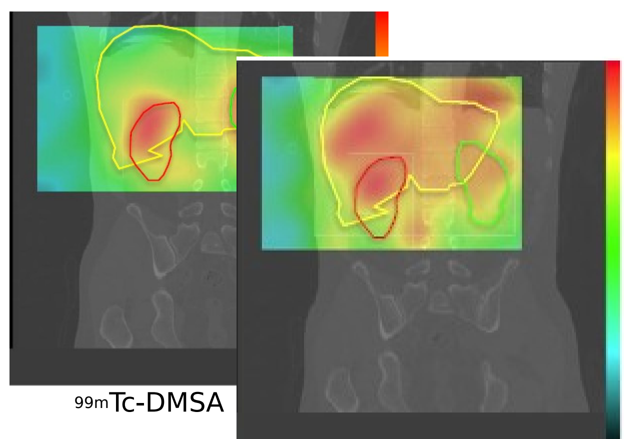

^{99m}Tc-DMSA

^{18}F-FDG

Takashi Nakano et al 2020 Phys. Med. Biol. 65 05LT01

Hadron therapy treatment monitoring

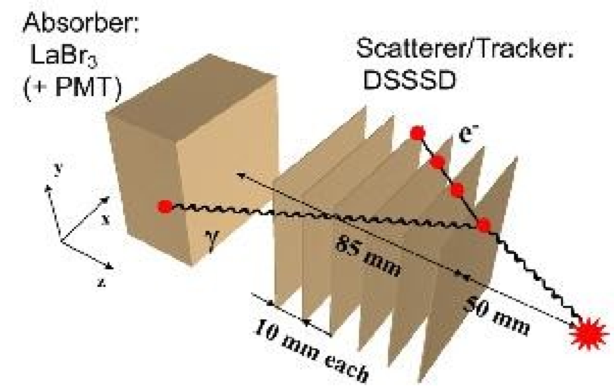

Peter Thirolf et al 2014 Med. Phy. 40(6)

Outline

- Introduction to Compton Cameras
- **MACACO Compton Camera**
- Application of Neural Networks to Enhance MACACO Compton Camera Imaging
  - Event Selection with Multi-Energy Radioactive Sources
  - Photon Interaction Localization in Monolithic Crystals
  - Background Reduction for Proton Range Verification
- Conclusions

MACACO III **M**edical **A**pplications **C**omp**A**ct **CO**mpton camera

- Monolithic $LaBr_3$ scintillator crystals of 25.8 x 25.8 mm^2 and 5 mm thickness.
- SiPM arrays S13360-3025CS from Hamamatsu photonics.
- MACACO III employs the ASIC VATA64HDR16 from IDEAS.
- AliVATA DAQ system developed by the group and commercialized by Alibava Systems S.L.

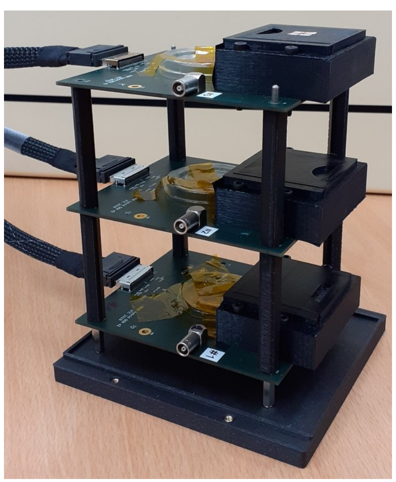

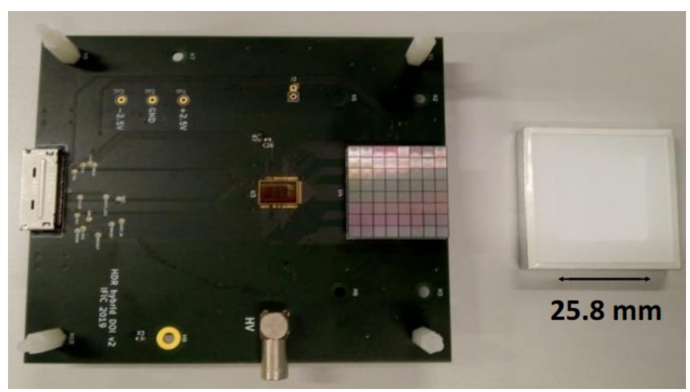

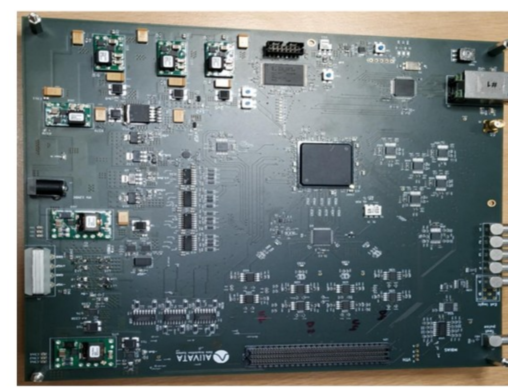

Outline

- Introduction to Compton Cameras
- MACACO Compton Camera
- **Application of Neural Networks to Enhance MACACO Compton Camera Imaging**
  - **Event Selection with Multi-Energy Radioactive Sources**
  - Photon Interaction Localization in Monolithic Crystals
  - Background Reduction for Proton Range Verification
- Conclusions

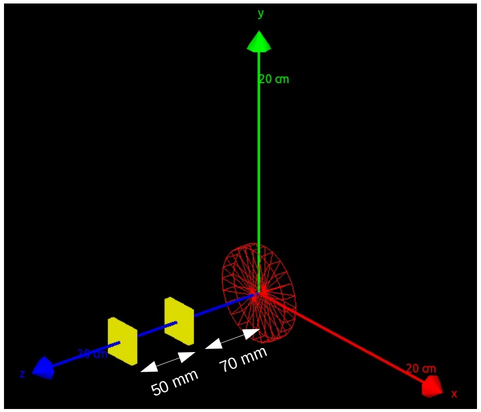

MACACO III simulation in Gate v8.2

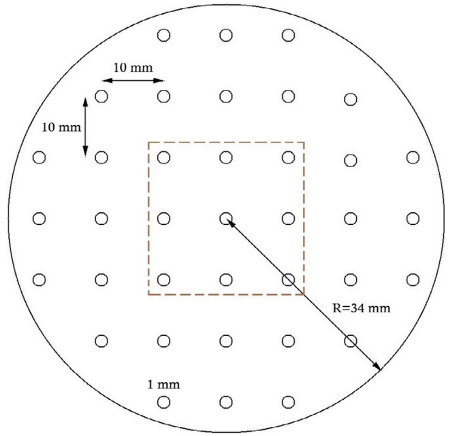

Array of 37 ^{22}Na sources

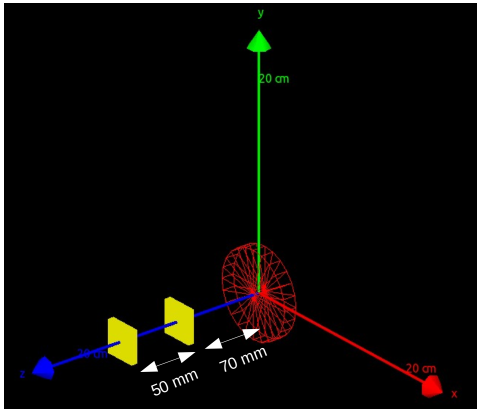

MACACO III simulation in Gate v8.2

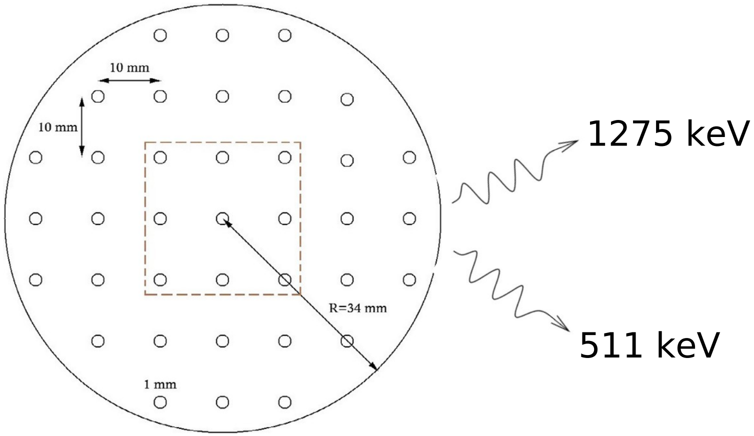

Array of 37 ^{22}Na sources

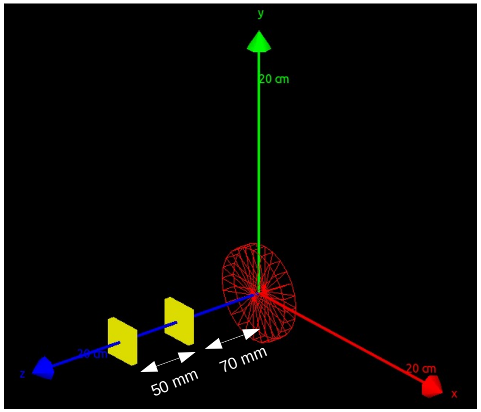

MACACO III simulation in Gate v8.2

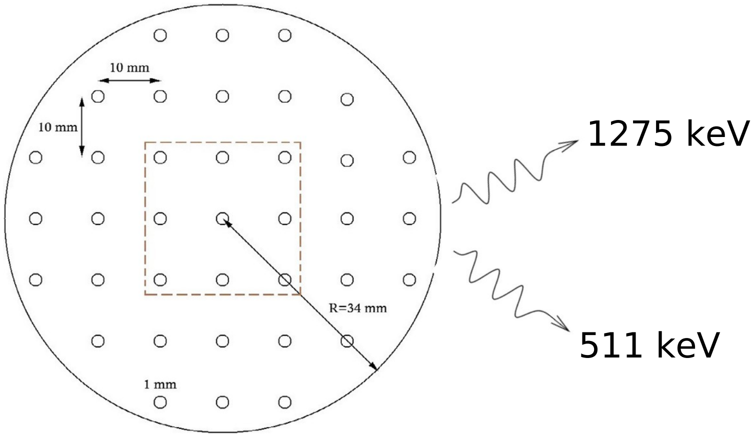

Array of 37 ^{22}Na sources

Data	Type
1275_good	0
511_good	1
1275_bs	1
511_bs	1
bad	1
unknown	1

Simulations

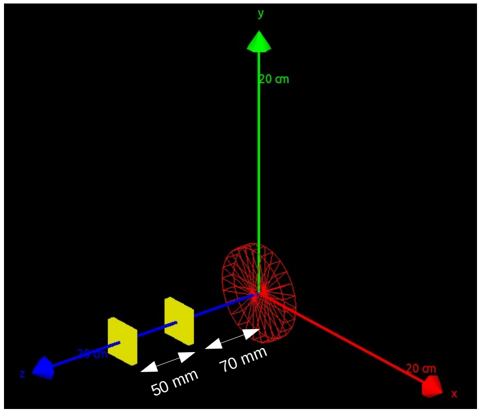

MACACO III simulation in Gate v8.2

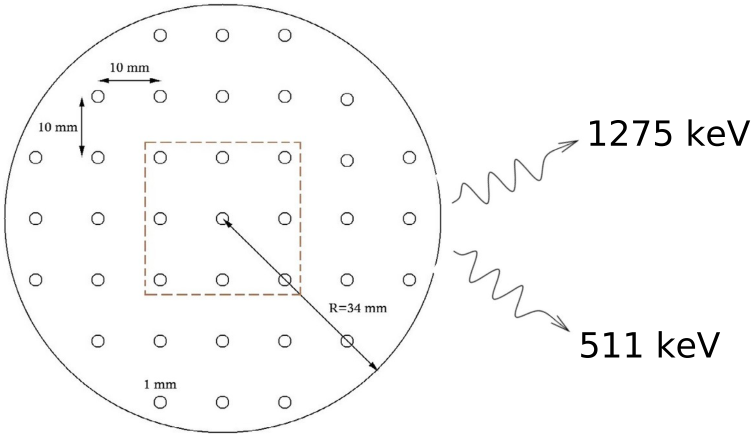

Array of 37 ^{22}Na sources

Data	Type
1275_good	0
511_good	1
1275_bs	1
511_bs	1
bad	1
unknown	1

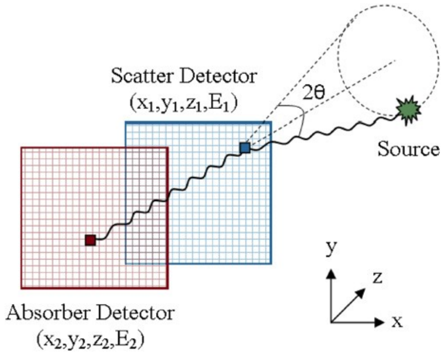

+

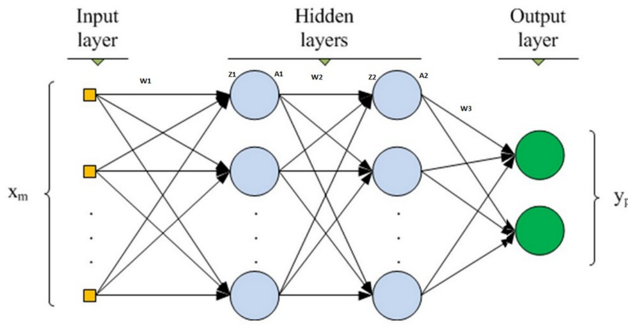

=

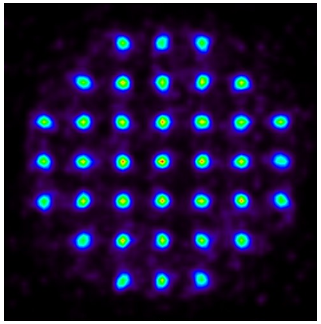

J. Pérez-Curbelo et al., Rad. Phys. and Chem (2024), https://doi.org/10.1016/j.radphyschem.2024.112166.

NNs trainning

Hyperparameters tuning by using Weights and Biases*

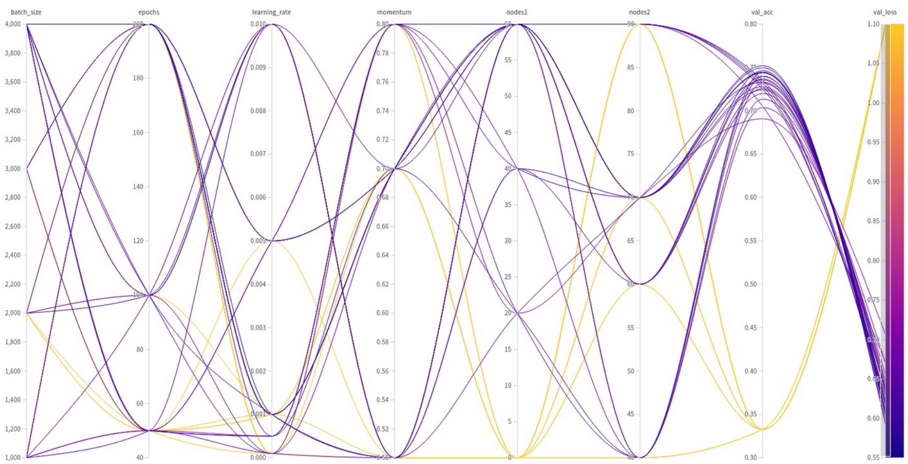

	NN
Layers (# of neurons)	1-6-1 (8-200-90-90-40-40-10-3)
Optimizer	Adam
Learning rate	0.001
Activation	ReLU sigmoid
Batch size	2000
Epoch	300

***L. Biewald. Weights & Biases. [Online]. Available: http://wandb .com.**

Experimental setup

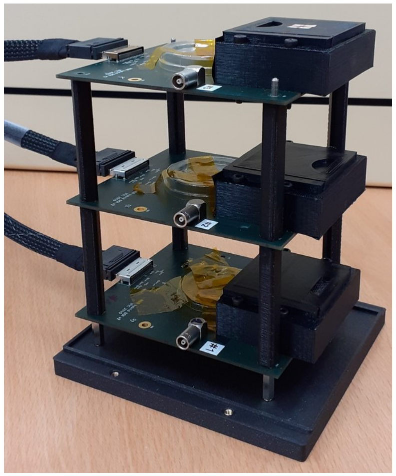

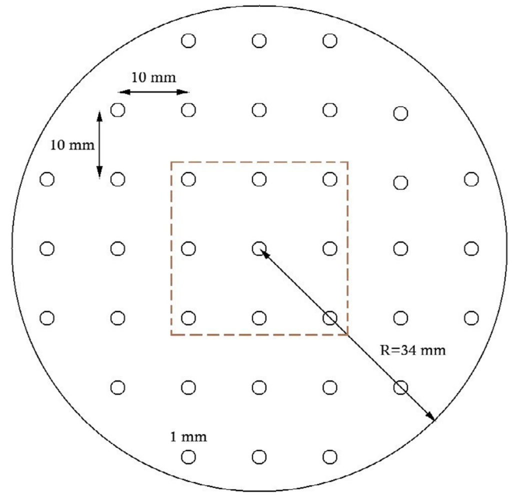

- 37 ^{22}Na sources
- 0.28 Mbq at the time of the measurement
- 21600 s

Experimental setup

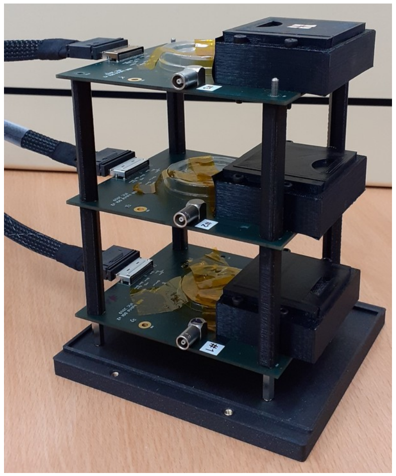

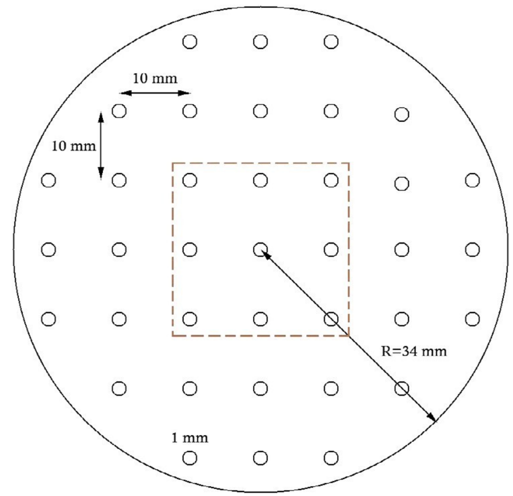

- 37 ^{22}Na sources
- 0.28 Mbq at the time of the measurement
- 21600 s

Deposited energy in the first plane
vs
Deposited energy in the second plane

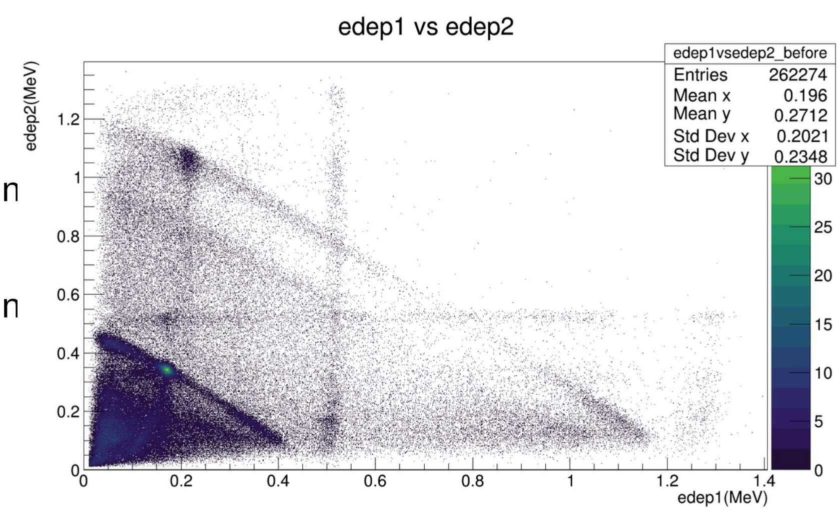

Data from coincidences in Plane 1 and Plane 2.

Experimental setup

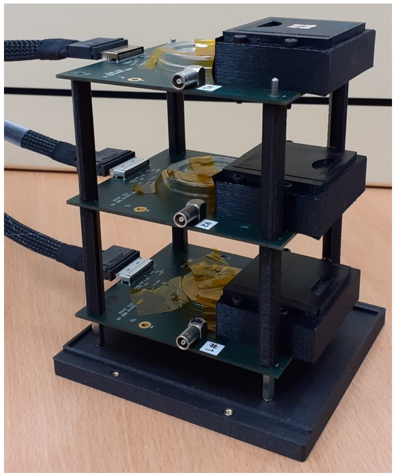

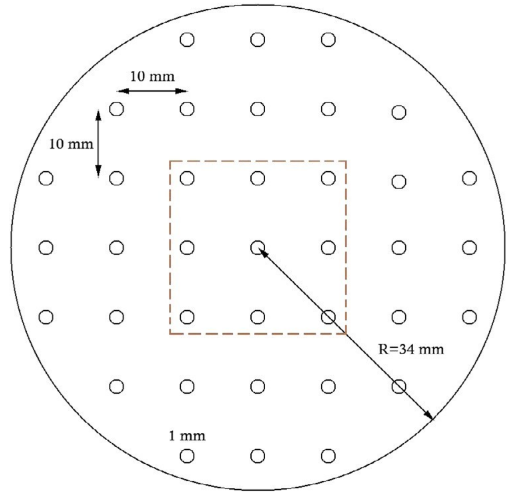

- 37 ^{22}Na sources
- 0.28 Mbq at the time of the measurement
- 21600 s

Deposited energy in the first plane
vs
Deposited energy in the second plane

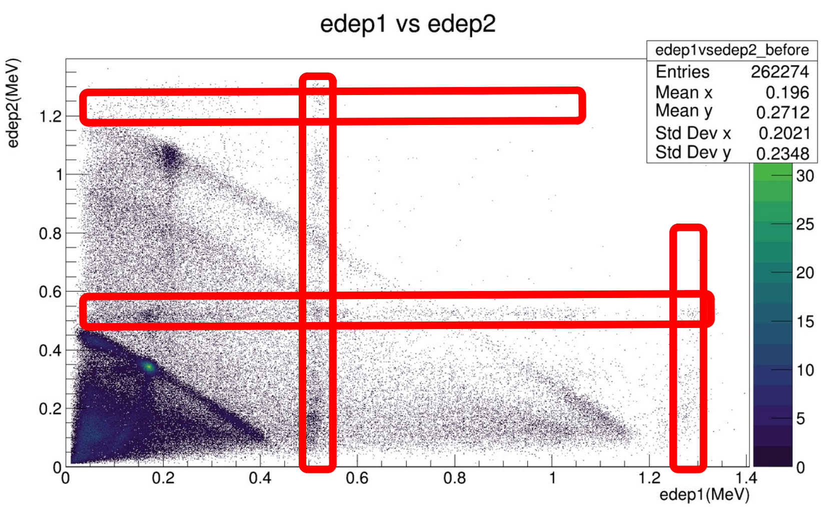

Random events

Data from coincidences in Plane 1 and Plane 2.

Experimental setup

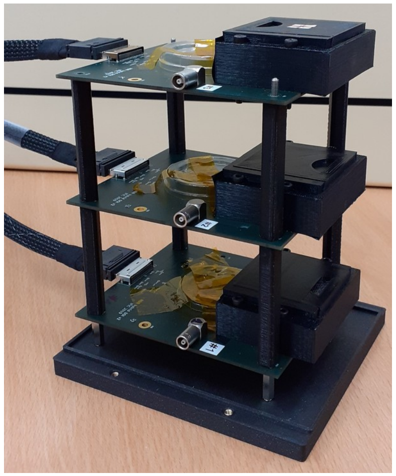

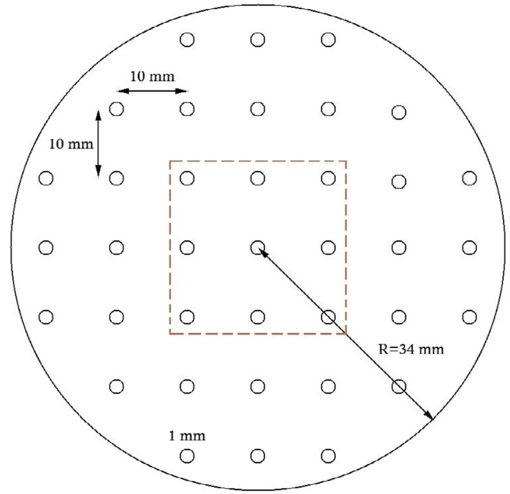

- 37 ^{22}Na sources
- 0.28 Mbq at the time of the measurement
- 21600 s

Deposited energy in the first plane
vs
Deposited energy in the second plane

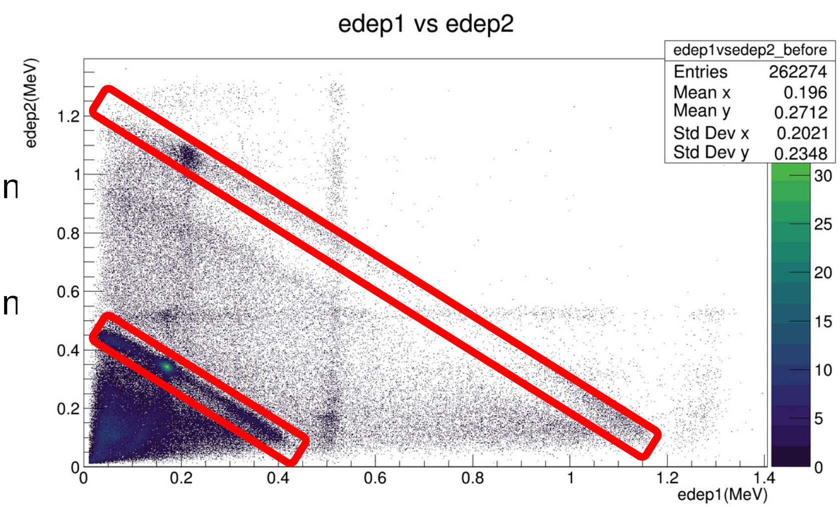

Total photon energy absorption

Data from coincidences in Plane 1 and Plane 2.

Experimental setup

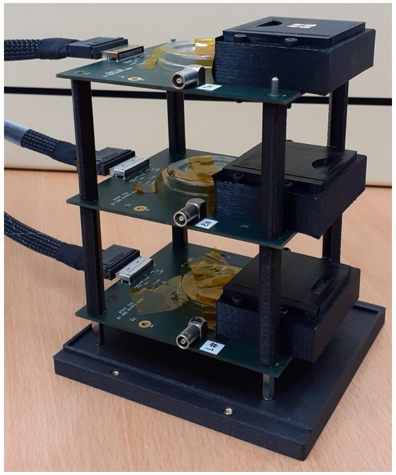

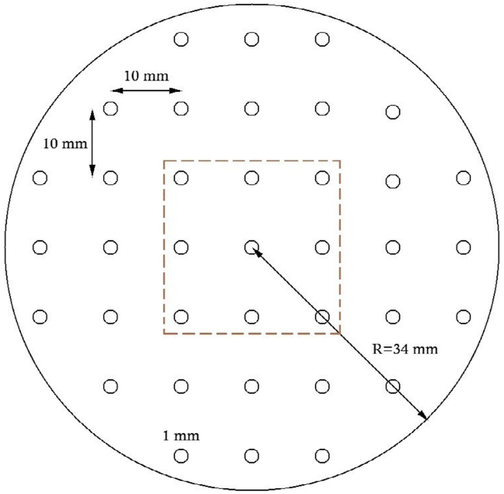

- 37 ^{22}Na sources
- 0.28 Mbq at the time of the measurement
- 21600 s

Deposited energy in the first plane vs Deposited energy in the second plane

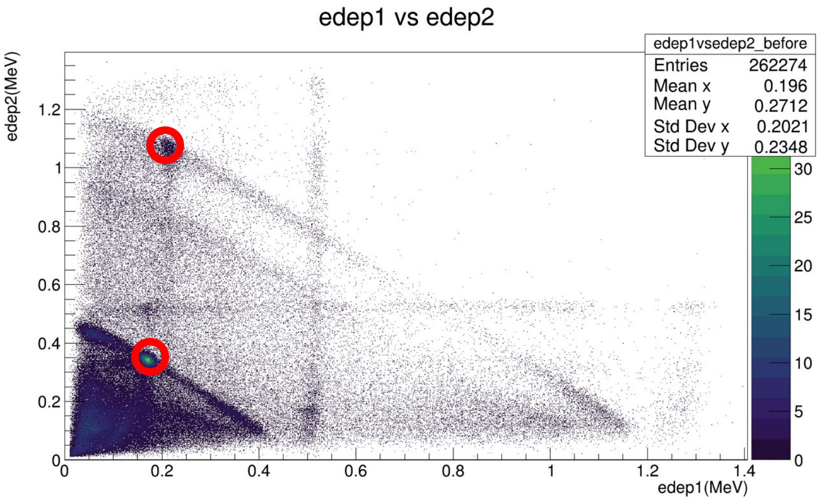

Backscatter events

Data from coincidences in Plane 1 and Plane 2.

Experimental setup

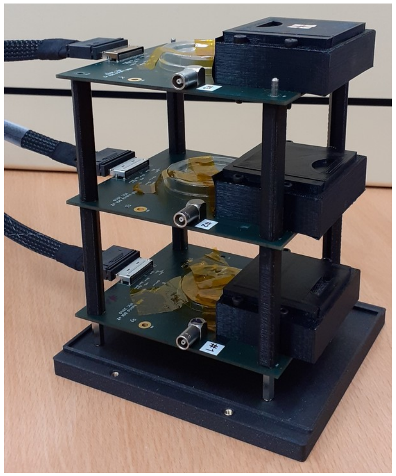

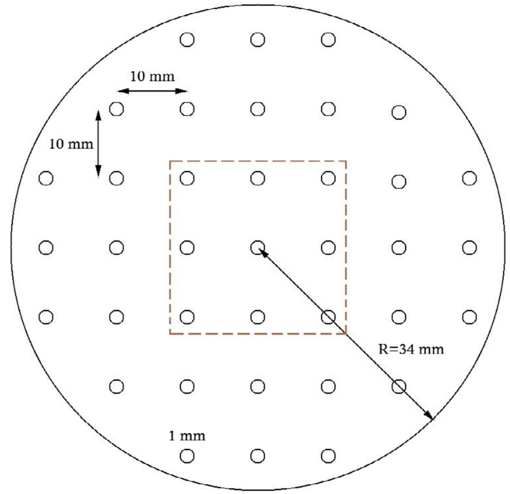

- 37 ^{22}Na sources
- 0.28 Mbq at the time of the measurement
- 21600 s

Deposited energy in the first plane vs Deposited energy in the second plane

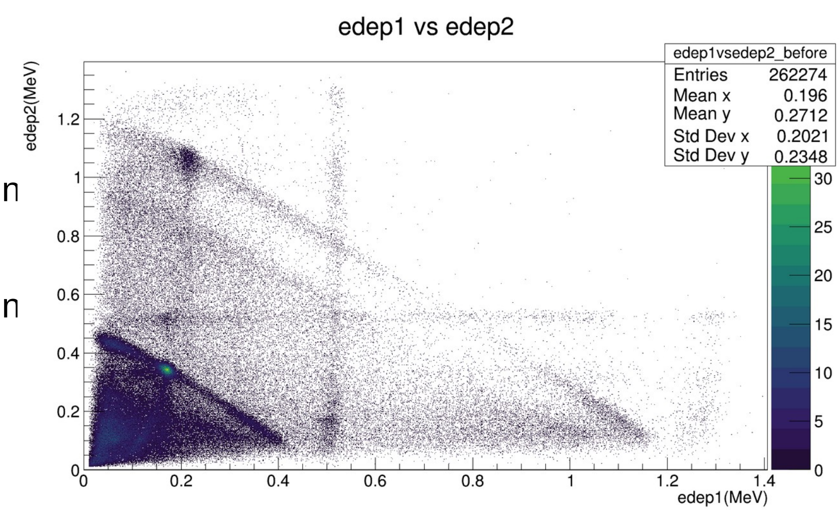

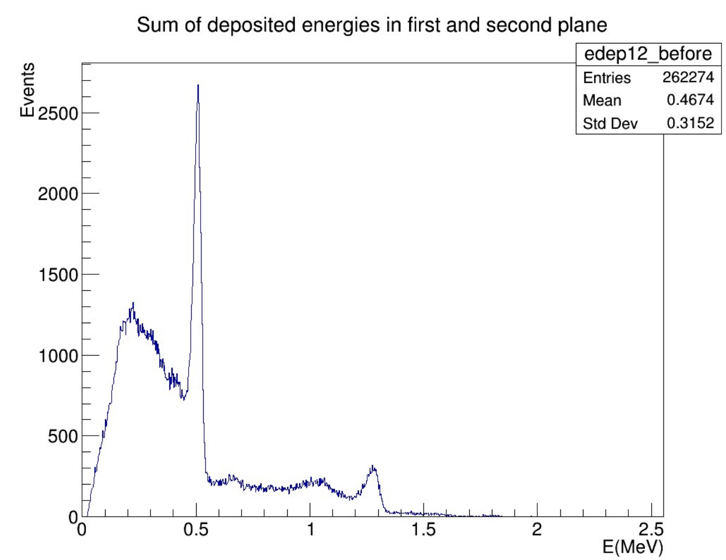

Data from coincidences in Plane 1 and Plane 2.

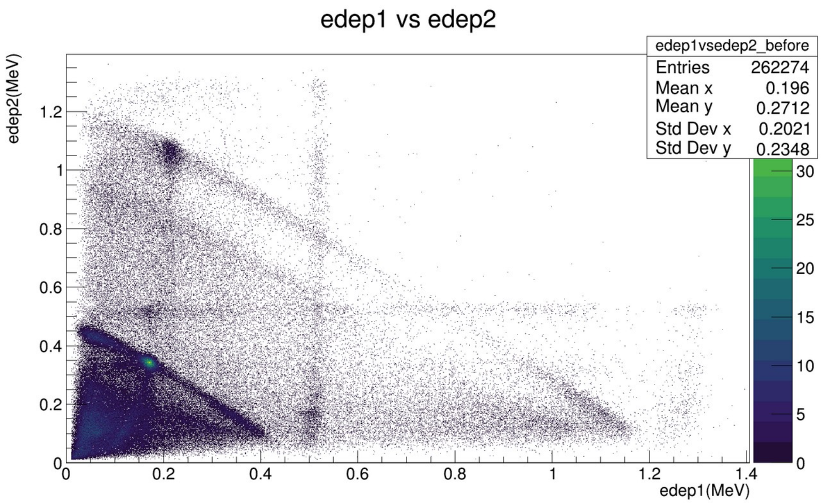

Deposited energy in the first plane vs Deposited energy in the second plane

NN selected data

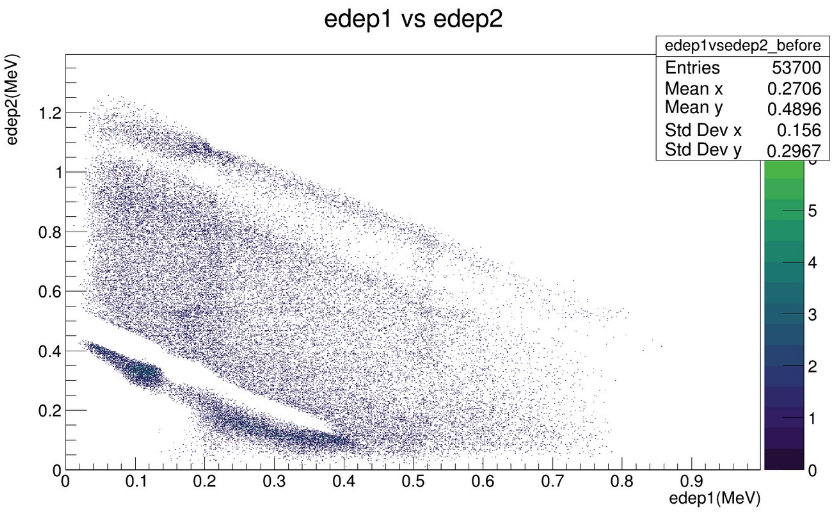

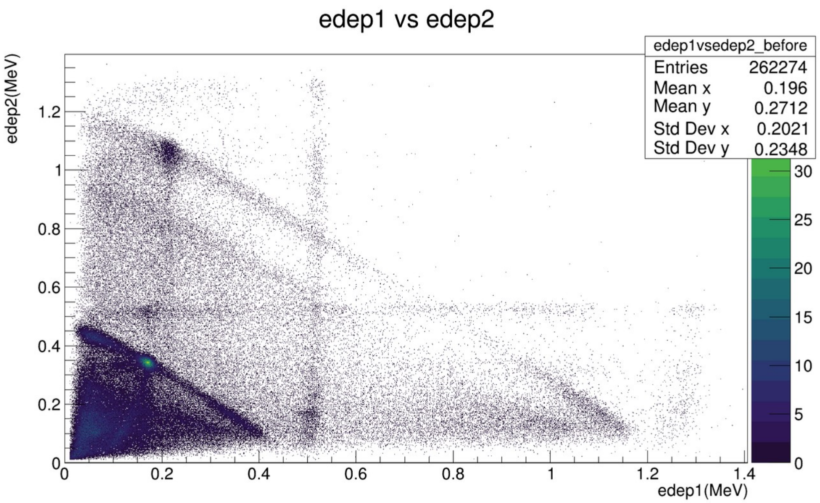

Deposited energy in the first plane vs Deposited energy in the second plane

NN selected data

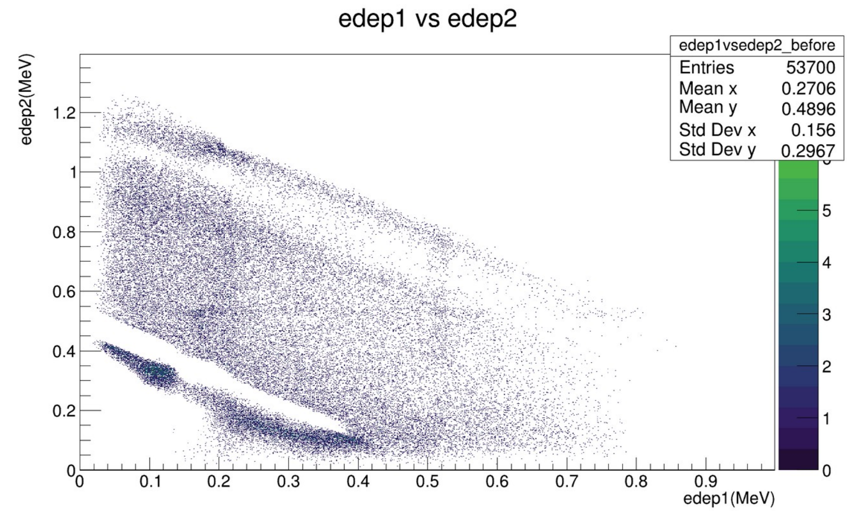

Energy cut method
Cut in 600 keV

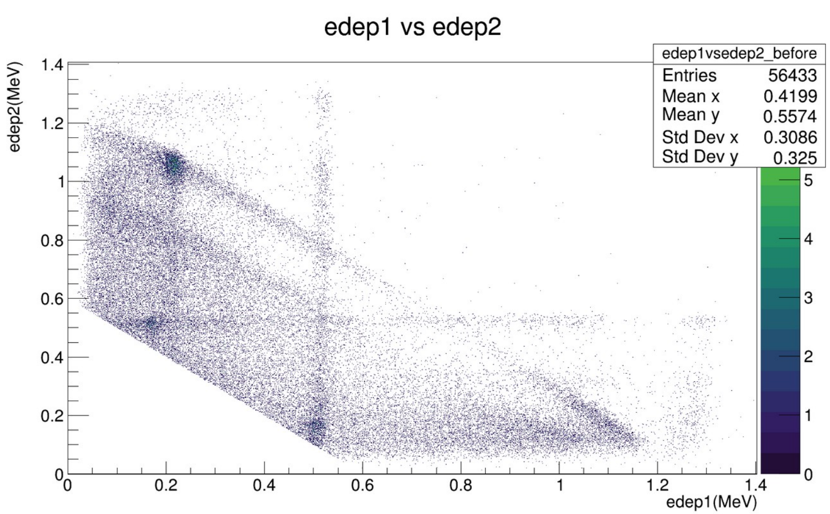

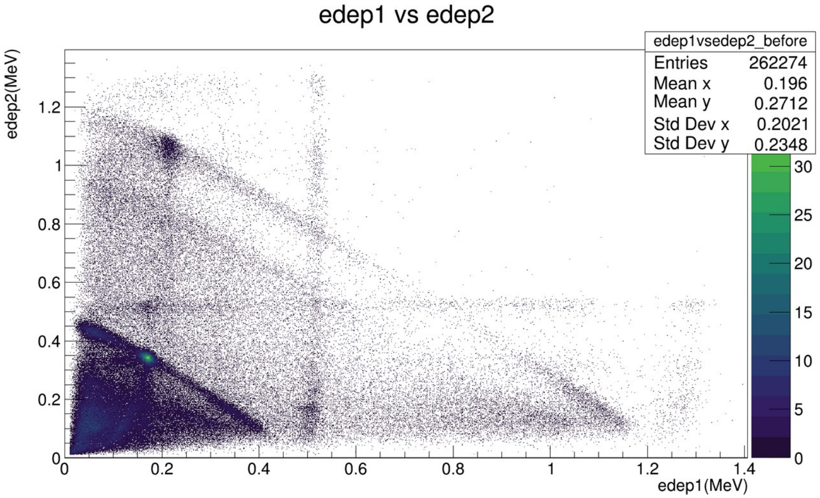

Deposited energy in the first plane
vs
Deposited energy in the second plane

NN selected data

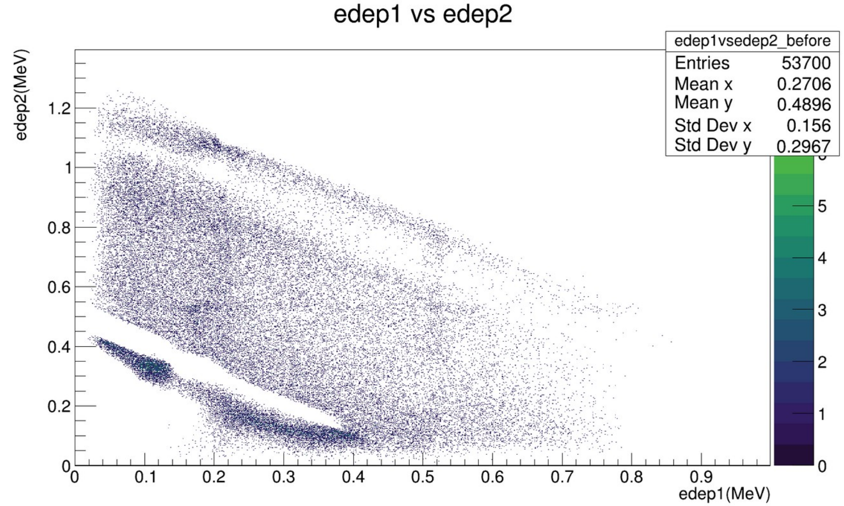

Energy cut method
Cut in 600 keV

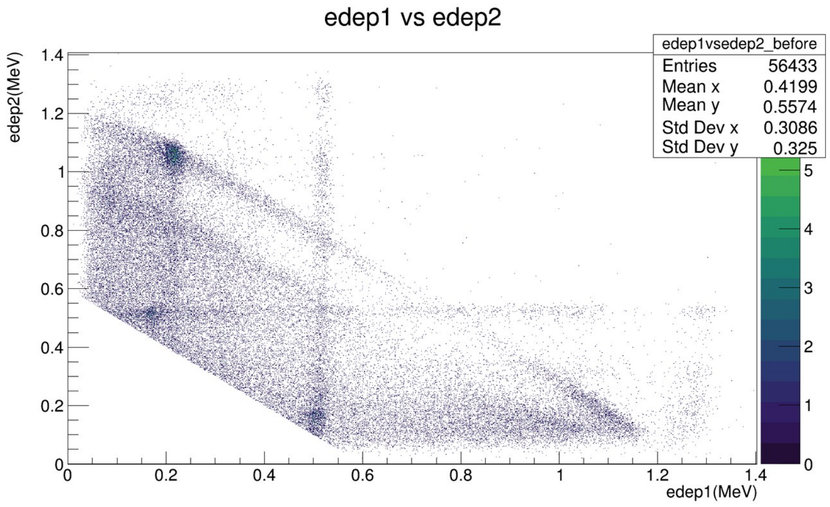

All experimental data

Experimental data selected by the two NNs

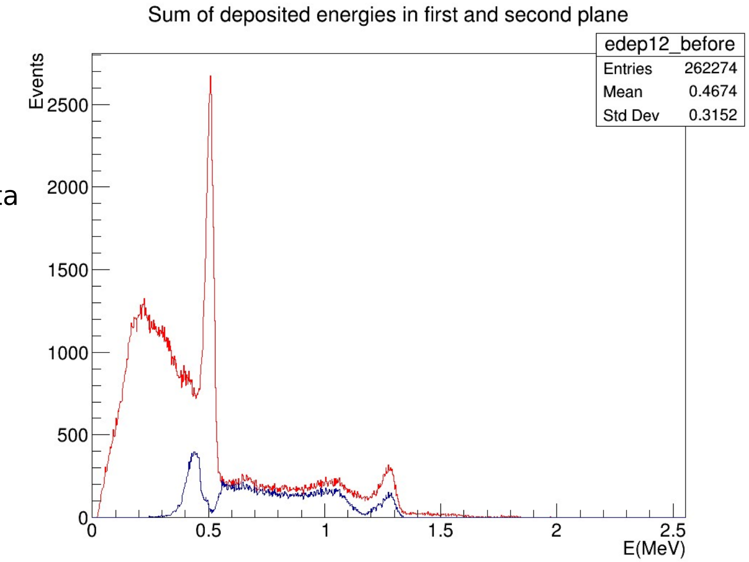

- Maximum Likelihood Expectation Maximization (MLEM) algorithm.
- System and sensitivity matrices are calculated analytically.*
- Median filter with 3×3×1 voxel window size.
- Field of View: 101×101×21 mm^3, volume grid composed by 1 mm^3 voxels.

*** E. Muñoz et al., Phys. Med. Biol., 2018, 63 (13): 135004.**

*** J. Roser et al., Phys. Med. Biol., 2020, 65, 145005.**

- Maximum Likelihood Expectation Maximization (MLEM) algorithm.
- System and sensitivity matrices are calculated analytically.*
- Median filter with 3×3×1 voxel window size.
- Field of View: 101×101×21 mm^3, volume grid composed by 1 mm^3 voxels.

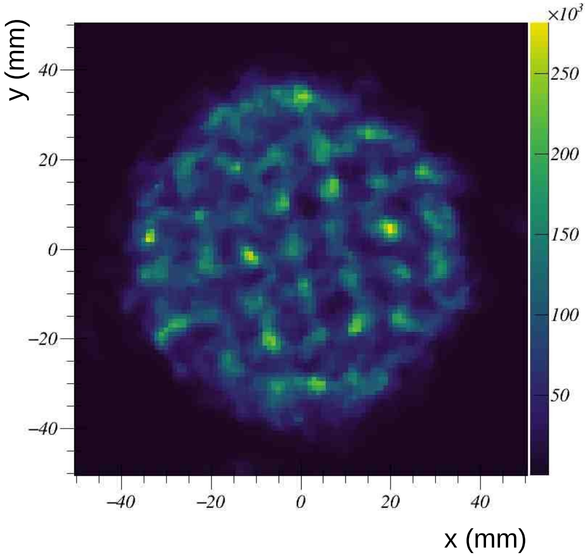

Image with good coincidences generated by 1275 keV photons classified by the two NNs.

*** E. Muñoz et al., Phys. Med. Biol., 2018, 63 (13): 135004.**

*** J. Roser et al., Phys. Med. Biol., 2020, 65, 145005.**

- Maximum Likelihood Expectation Maximization (MLEM) algorithm.
- System and sensitivity matrices are calculated analytically.*
- Median filter with 3×3×1 voxel window size.
- Field of View: 101×101×21 mm^3, volume grid composed by 1 mm^3 voxels.

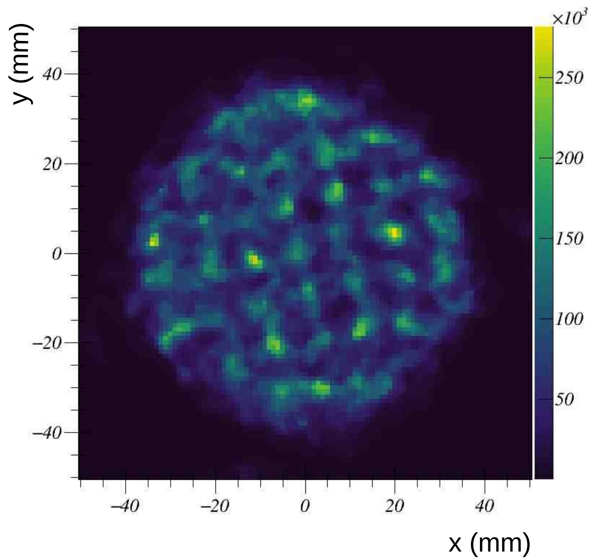

Image with good coincidences generated by 1275 keV photons classified by the two NNs.

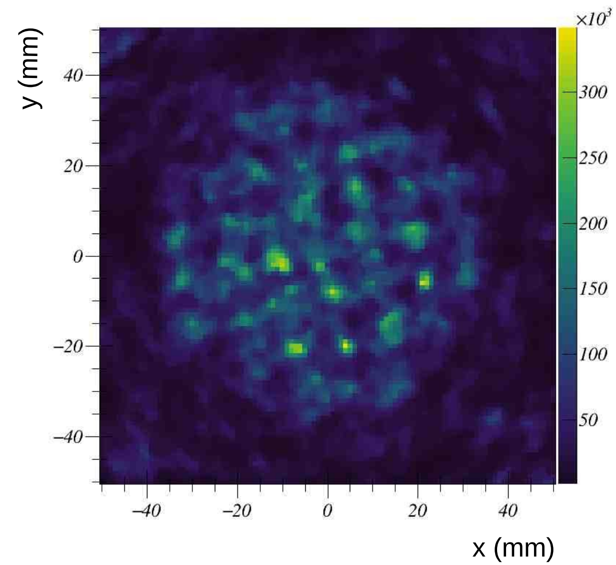

Image with all experimental events applying a cut in 600 keV prior to reconstruction.

*** E. Muñoz et al., Phys. Med. Biol., 2018, 63 (13): 135004.**

*** J. Roser et al., Phys. Med. Biol., 2020, 65, 145005.**

Image with good coincidences generated by 1275 keV photons classified by the two NNs.

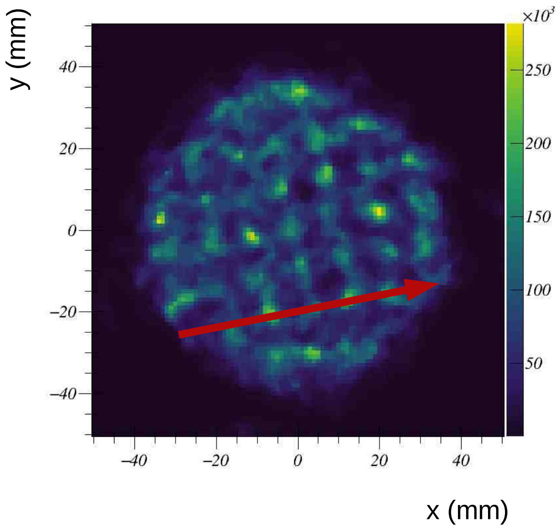

Image with all experimental events applying a cut in 600 keV prior to reconstruction.

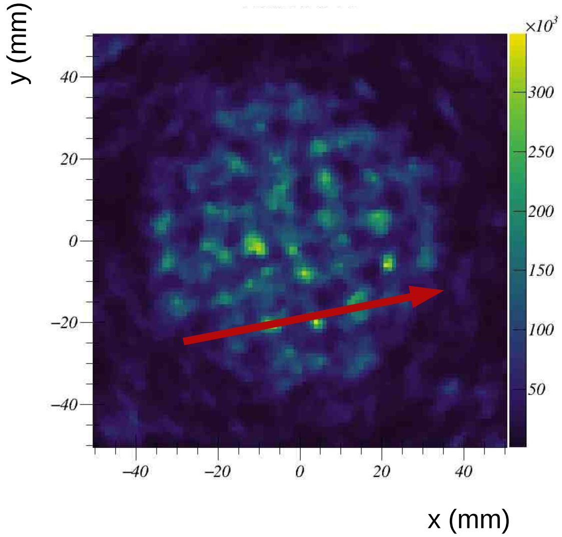

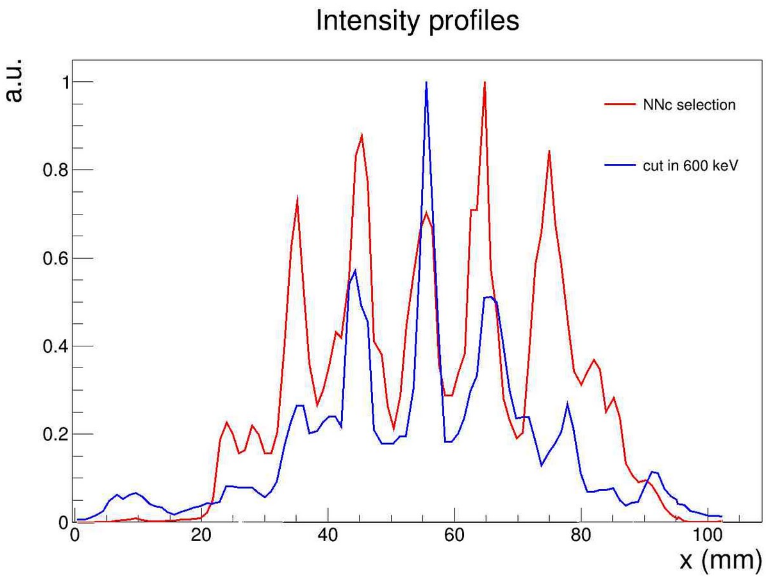

Outline

- Introduction to Compton Cameras
- MACACO Compton Camera
- **Application of Neural Networks to Enhance MACACO Compton Camera Imaging**
  - Event Selection with Multi-Energy Radioactive Sources
  - **Photon Interaction Localization in Monolithic Crystals**
  - Background Reduction for Proton Range Verification
- Conclusions

- Maximum Likelihood Expectation Maximization (MLEM) algorithm.
- System and sensitivity matrices are calculated analytically.

Image reconstruction for a multi-layer Compton telescope: an analytical model for three interaction events

J Roser[1], E Muñoz[1], L Barrientos[1], J Barrio[1], J Bernabéu[1], M Borja-Lloret[1], A Etxebeste[1], G Llosá[1], A Ros[1], R Viegas[1] + Show full author list

Published 8 July 2020 • © 2020 Institute of Physics and Engineering in Medicine

Physics in Medicine & Biology, Volume 65, Number 14

Citation J Roser *et al* 2020 *Phys. Med. Biol.* **65** 145005

Study and comparison of different sensitivity models for a two-plane Compton camera

Enrique Muñoz[1], John Barrio[1], José Bernabéu[1], Ane Etxebeste[1], Carlos Lacasta[1], Gabriela Llosá[1], Ana Ros[1], Jorge Roser[1] and Josep F Oliver[1]

Published 25 June 2018 • © 2018 Institute of Physics and Engineering in Medicine

Physics in Medicine & Biology, Volume 63, Number 13

Citation Enrique Muñoz *et al* 2018 *Phys. Med. Biol.* **63** 135004

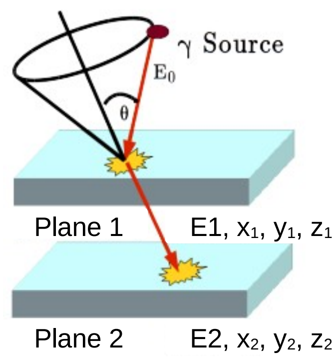

$$cos\theta = 1 - mc^2\left(\frac{1}{E_0 - \tilde{E}_1} - \frac{1}{E_0}\right)$$

- Maximum Likelihood Expectation Maximization (MLEM) algorithm.
- System and sensitivity matrices are calculated analytically.

Image reconstruction for a multi-layer Compton telescope: an analytical model for three interaction events

J Roser[1], E Muñoz[1], L Barrientos[1], J Barrio[1], J Bernabéu[1], M Borja-Lloret[1], A Etxebeste[1], G Llosá[1], A Ros[1], R Viegas[1] + Show full author list

Published 8 July 2020 • © 2020 Institute of Physics and Engineering in Medicine

Physics in Medicine & Biology, Volume 65, Number 14

Citation J Roser *et al* 2020 *Phys. Med. Biol.* **65** 145005

Study and comparison of different sensitivity models for a two-plane Compton camera

Enrique Muñoz[1], John Barrio[1], José Bernabéu[1], Ane Etxebeste[1], Carlos Lacasta[1], Gabriela Llosá[1], Ana Ros[1], Jorge Roser[1] and Josep F Oliver[1]

Published 25 June 2018 • © 2018 Institute of Physics and Engineering in Medicine

Physics in Medicine & Biology, Volume 63, Number 13

Citation Enrique Muñoz *et al* 2018 *Phys. Med. Biol.* **63** 135004

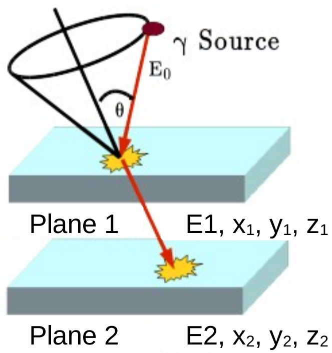

$$cos\theta = 1 - mc^2 \left(\frac{1}{E_0 - \tilde{E}_1} - \frac{1}{E_0} \right)$$

Analytical method

IOP Publishing | Institute of Physics and Engineering in Medicine — Physics in Medicine & Biology

Phys. Med. Biol. **61** (2016) 3914–3934 — doi:10.1088/0031-9155/61/10/3914

3D position determination in monolithic crystals coupled to SiPMs for PET

Ane Etxebeste, John Barrio, Enrique Muñoz, Josep F Oliver, Carles Solaz and Gabriela Llosá

Instituto de Física Corpuscular, CSIC/Universitat de València, Valencia, Spain

E-mail: ane.etxebeste@ific.uv.es

Received 20 November 2015, revised 29 February 2016
Accepted for publication 29 March 2016
Published 27 April 2016

CrossMark

Abstract

The interest in using continuous monolithic crystals in positron emission tomography (PET) has grown in the last years. Coupled to silicon photomultipliers (SiPMs), the detector can combine high sensitivity and high resolution, the two main factors to be maximized in a positron emission tomograph. In this work, the position determination capability of a detector comprised of a $12 \times 12 \times 10$ mm^3 LYSO crystal coupled to an 8×8-pixel array of SiPMs is evaluated. The 3D interaction position of γ-rays is estimated using an analytical model of the light distribution including reflections on the facets of the crystal. Monte Carlo simulations have been performed to evaluate different crystal reflectors and geometries. The method has been characterized and applied to different cases. Intrinsic resolution obtained with the position estimation method used in this work, applied to experimental data, achieves sub-millimetre resolution values. Average resolution over the detector surface for 5 mm thick crystal is ~0.9 mm FWHM and ~1.2 mm FWHM for 10 mm thick crystal. Depth of interaction resolution is close to 2 mm FWHM in both cases, while the FWTM is ~5.3 mm for 5 mm thick crystal and ~9.6 mm for 10 mm thick crystal.

Keywords: monolithic crystal, silicon photomultiplier, depth of interaction

Introduction

- Maximum Likelihood Expectation Maximization (MLEM) algorithm.
- System and sensitivity matrices are calculated analytically.

Image reconstruction for a multi-layer Compton telescope: an analytical model for three interaction events

J Roser[1], E Muñoz[1], L Barrientos[1], J Barrio[1], J Bernabéu[1], M Borja-Lloret[1], A Etxebeste[1], G Llosá[1], A Ros[1], R Viegas[1] + Show full author list

Published 8 July 2020 • © 2020 Institute of Physics and Engineering in Medicine
Physics in Medicine & Biology, Volume 65, Number 14
Citation J Roser *et al* 2020 *Phys. Med. Biol.* **65** 145005

Study and comparison of different sensitivity models for a two-plane Compton camera

Enrique Muñoz[1], John Barrio[1], José Bernabéu[1], Ane Etxebeste[1], Carlos Lacasta[1], Gabriela Llosá[1], Ana Ros[1], Jorge Roser[1] and Josep F Oliver[1]

Published 25 June 2018 • © 2018 Institute of Physics and Engineering in Medicine
Physics in Medicine & Biology, Volume 63, Number 13
Citation Enrique Muñoz *et al* 2018 *Phys. Med. Biol.* **63** 135004

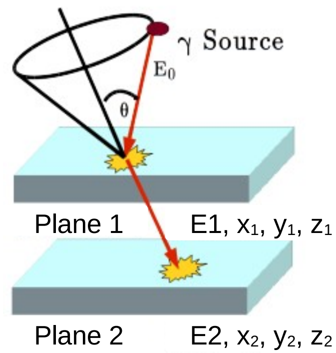

$$cos\theta = 1 - mc^2\left(\frac{1}{E_0 - \tilde{E}_1} - \frac{1}{E_0}\right)$$

Analytical method

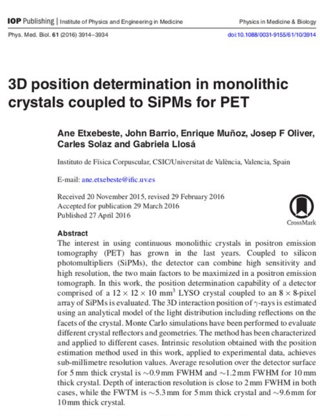

IOP Publishing | Institute of Physics and Engineering in Medicine — Physics in Medicine & Biology

Phys. Med. Biol. 61 (2016) 3914–3934 — doi:10.1088/0031-9155/61/10/3914

3D position determination in monolithic crystals coupled to SiPMs for PET

Ane Etxebeste, John Barrio, Enrique Muñoz, Josep F Oliver, Carles Solaz and Gabriela Llosá

Instituto de Física Corpuscular, CSIC/Universitat de València, Valencia, Spain

E-mail: ane.etxebeste@ific.uv.es

Received 20 November 2015, revised 29 February 2016
Accepted for publication 29 March 2016
Published 27 April 2016

Abstract
The interest in using continuous monolithic crystals in positron emission tomography (PET) has grown in the last years. Coupled to silicon photomultipliers (SiPMs), the detector can combine high sensitivity and high resolution, the two main factors to be maximized in a positron emission tomograph. In this work, the position determination capability of a detector comprised of a 12 × 12 × 10 mm³ LYSO crystal coupled to an 8 × 8-pixel array of SiPMs is evaluated. The 3D interaction position of γ-rays is estimated using an analytical model of the light distribution including reflections on the facets of the crystal. Monte Carlo simulations have been performed to evaluate different crystal reflectors and geometries. The method has been characterized and applied to different cases. Intrinsic resolution obtained with the position estimation method used in this work, applied to experimental data, achieves sub-millimetre resolution values. Average resolution over the detector surface for 5 mm thick crystal is ~0.9 mm FWHM and ~1.2 mm FWHM for 10 mm thick crystal. Depth of interaction resolution is close to 2 mm FWHM in both cases, while the FWTM is ~5.3 mm for 5 mm thick crystal and ~9.6 mm for 10 mm thick crystal.

Keywords: monolithic crystal, silicon photomultiplier, depth of interaction

Neural networks method

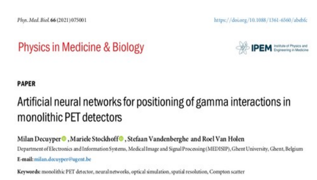

Phys. Med. Biol. 66 (2021) 075001 — https://doi.org/10.1088/1361-6560/abebfc

Physics in Medicine & Biology — IPEM

PAPER

Artificial neural networks for positioning of gamma interactions in monolithic PET detectors

Milan Decuyper, Mariele Stockhoff, Stefaan Vandenberghe and Roel Van Holen

Department of Electronics and Information Systems, Medical Image and Signal Processing (MEDISIP), Ghent University, Ghent, Belgium

E-mail: milan.decuyper@ugent.be

Keywords: monolithic PET detector, neural networks, optical simulation, spatial resolution, Compton scatter

Contents lists available at ScienceDirect

Nuclear Instruments and Methods in Physics Research A

journal homepage: www.elsevier.com/locate/nima

Localisation of gamma-ray interaction points in thick monolithic $CeBr_3$ and $LaBr_3$:Ce scintillators

Alexei Ulyanov[a,*], Oran Morris[a,b], Oliver J. Roberts[a], Isaac Tobin[a], Lorraine Hanlon[a], Sheila McBreen[a], David Murphy[a], Nick Nelms[c], Brian Shortt[c]

[a] School of Physics, University College Dublin, Belfield, Dublin 4, Ireland
[b] Department of Computer Science & Applied Physics, Galway-Mayo Institute of Technology, Galway, Ireland
[c] European Space Agency, ESTEC, 2200 AG Noordwijk, The Netherlands

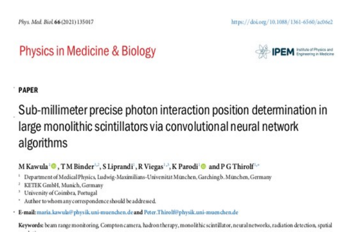

Phys. Med. Biol. 66 (2021) 135017 — https://doi.org/10.1088/1361-6560/ac06e2

Physics in Medicine & Biology — IPEM

PAPER

Sub-millimeter precise photon interaction position determination in large monolithic scintillators via convolutional neural network algorithms

M Kawula[1,*], T M Binder[1,2], S Liprandi[1], R Viegas[1,3], K Parodi[1] and P G Thirolf[1,*]

[1] Department of Medical Physics, Ludwig-Maximilians-Universität München, Garching b. München, Germany
[2] KETEK GmbH, Munich, Germany
[3] University of Coimbra, Portugal
[*] Author to whom any correspondence should be addressed.

E-mail: maria.kawula@physik.uni-muenchen.de and Peter.Thirolf@physik.uni-muenchen.de

Keywords: beam range monitoring, Compton camera, hadrontherapy, monolithic scintillator, neural networks, radiation detection, spatial resolution

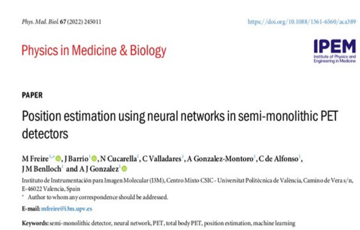

Phys. Med. Biol. 67 (2022) 245011 — https://doi.org/10.1088/1361-6560/aca389

Physics in Medicine & Biology — IPEM

PAPER

Position estimation using neural networks in semi-monolithic PET detectors

M Freire[1,*], J Barrio[1], N Cucarella[1], C Valladares[1], A Gonzalez-Montoro[1], C de Alfonso[1], J M Benlloch[1] and A J Gonzalez[1]

Instituto de Instrumentación para Imagen Molecular (I3M), Centro Mixto CSIC - Universitat Politècnica de València, Camino de Vera s/n, E-46022 Valencia, Spain
[*] Author to whom any correspondence should be addressed.

E-mail: mfreire@i3m.upv.es

Keywords: semi-monolithic detector, neural network, PET, total body PET, position estimation, machine learning

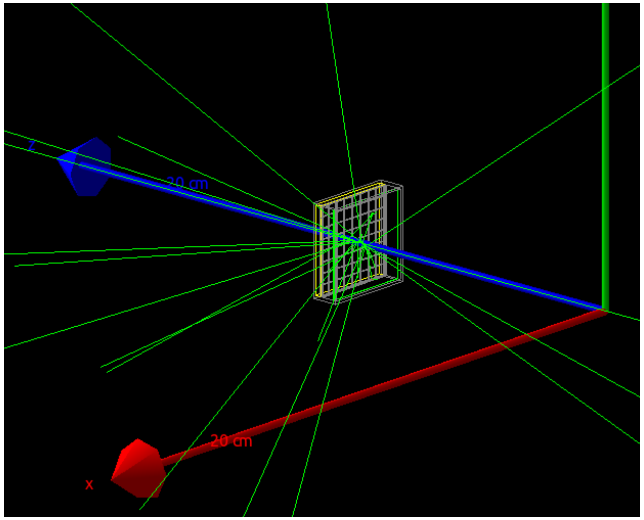

MACACO III simulation in Gate v7.0

- Realistic simulations:
  - One plane of MACACO III.
  - 25.8 × 25.8 × 5 mm^3 $LaBr_3$ scintillator crystal.
  - 8 × 8 SiPM array with a pixel size of 3 × 3 mm^2.
  - Perpendicular 511 keV pencil beam.

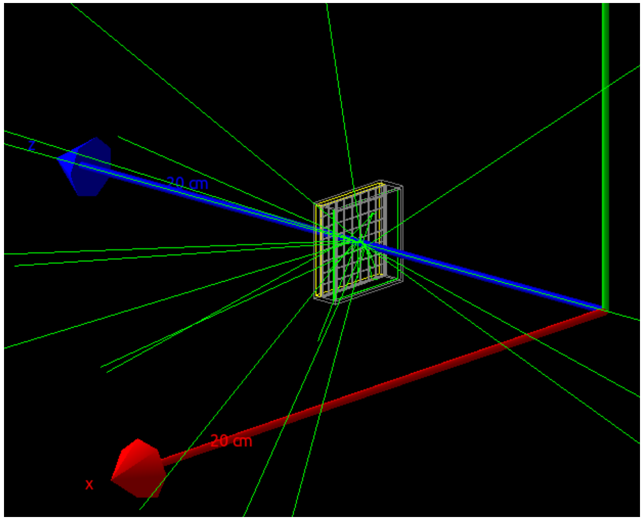

MACACO III simulation in Gate v7.0

- Realistic simulations:
  - One plane of MACACO III.
  - 25.8 × 25.8 × 5 mm³ $LaBr_3$ scintillator crystal.
  - 8 × 8 SiPM array with a pixel size of 3 × 3 mm².
  - Perpendicular 511 keV pencil beam.

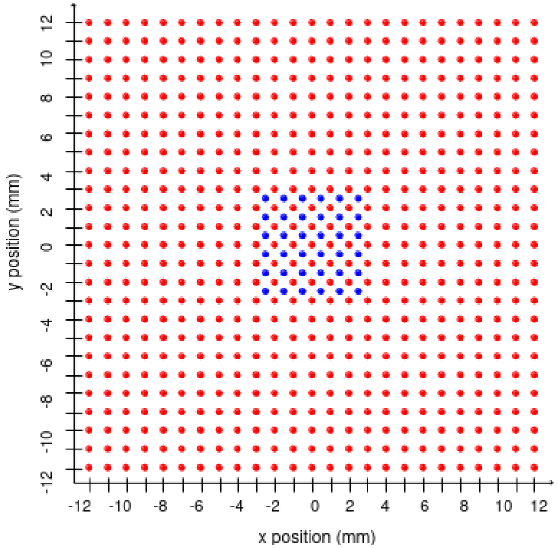

- 12 × 12 grid, 1 mm step.
  - 6000 events per position for training.
  - 2000 events per position for testing.
- 6 × 6 grid, 0.5 mm step.
  - 2000 events per position for validating and avoiding overfitting.

Two grid sweeps for model training, validating and testing

NNs trainning

- The light collected by each pixel of the SiPM was used to create an 8 × 8 image for training the CNN model.

x = 3.0   y = 3.0

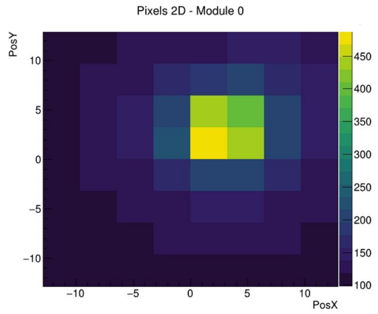

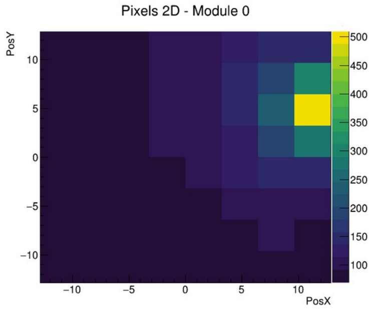

x = 12.0   y = 5.0

NNs trainning

- The light collected by each pixel of the SiPM was used to create an 8 × 8 image for training the CNN model.

x = 3.0 y = 3.0

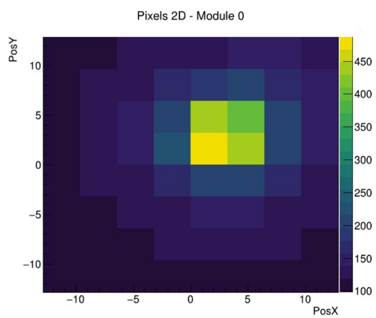

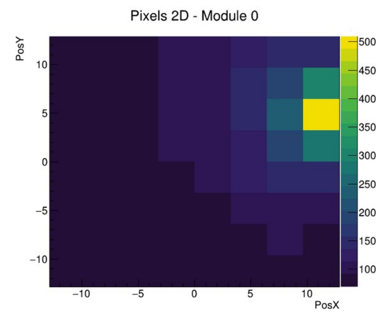

x = 12.0 y = 5.0

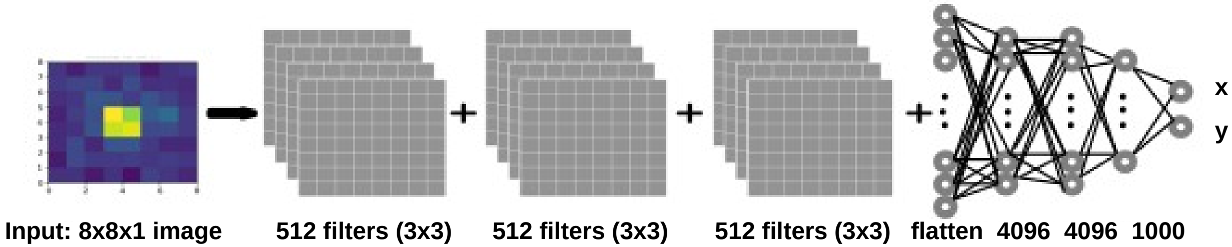

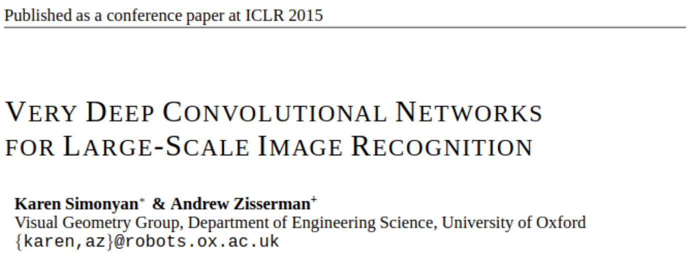

Published as a conference paper at ICLR 2015

VERY DEEP CONVOLUTIONAL NETWORKS FOR LARGE-SCALE IMAGE RECOGNITION

Karen Simonyan* & Andrew Zisserman+
Visual Geometry Group, Department of Engineering Science, University of Oxford
{karen,az}@robots.ox.ac.uk

NNs trainning

- The light collected by each pixel of the SiPM was used to create an 8 × 8 image for training the CNN model.

x = 3.0 y = 3.0

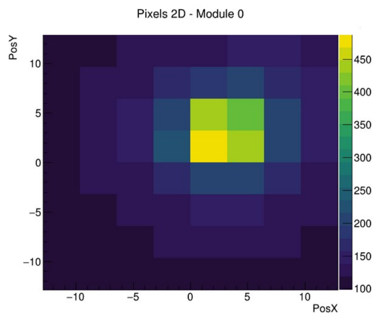

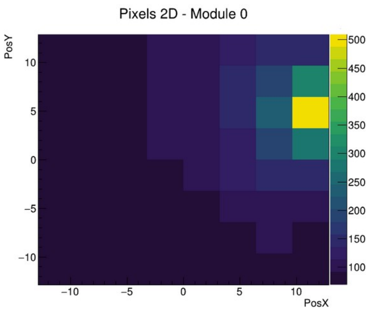

x = 12.0 y = 5.0

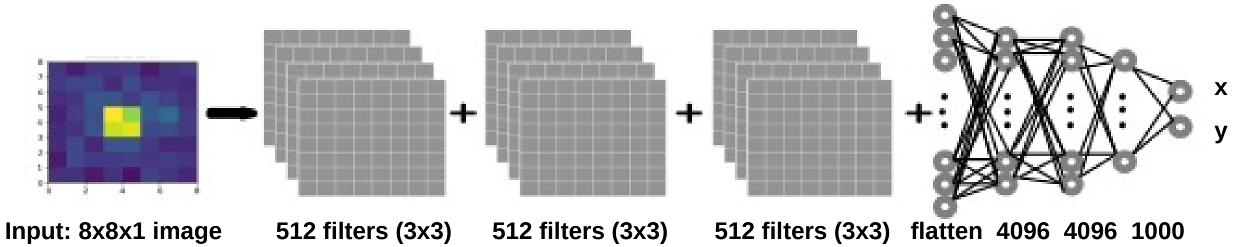

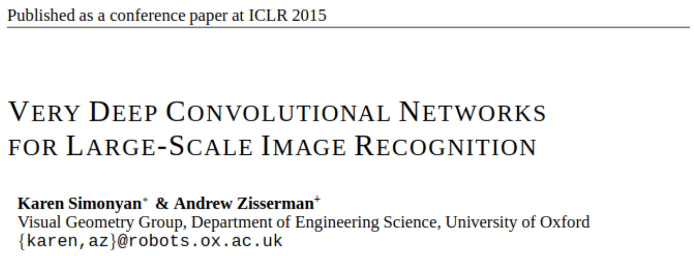

Published as a conference paper at ICLR 2015

VERY DEEP CONVOLUTIONAL NETWORKS FOR LARGE-SCALE IMAGE RECOGNITION

Karen Simonyan* & Andrew Zisserman+
Visual Geometry Group, Department of Engineering Science, University of Oxford
{karen,az}@robots.ox.ac.uk

- Ground truth: positions provided by Gate.
- Loss function: Mean absolute error (MAE).
- Optimizer: Adam.

- MAE, euclidean distance and the full width at half maximun (FWHM) as figures of merit (FOMs).
- Once the 2D model was trained, it was used to predict the depth of interaction (DOI).

Results

Difference real - predicted in *x* direction

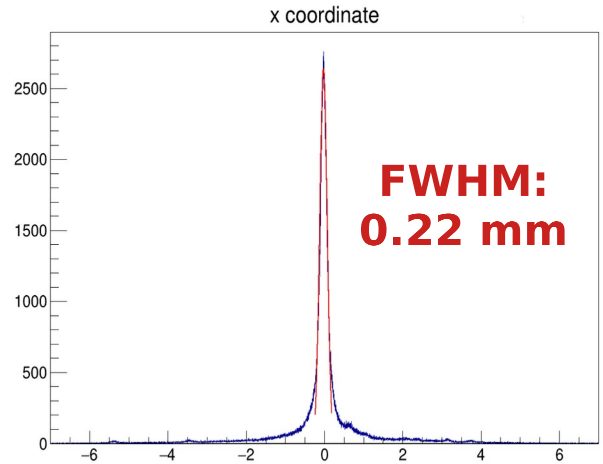

Same result for the y direction

2D Error distribution

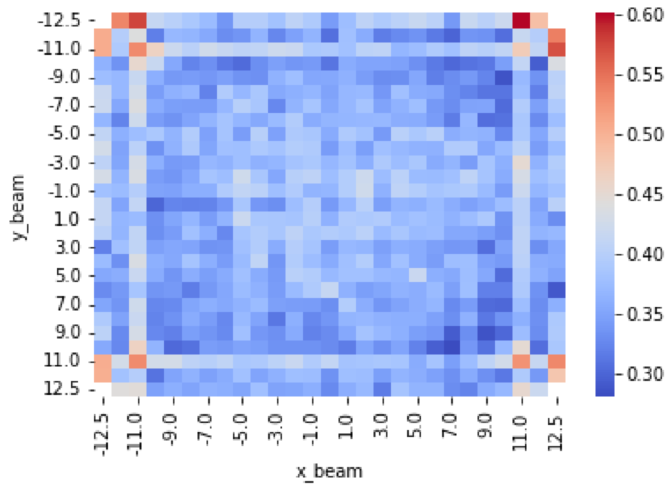

Results

Difference real - predicted in *x* direction

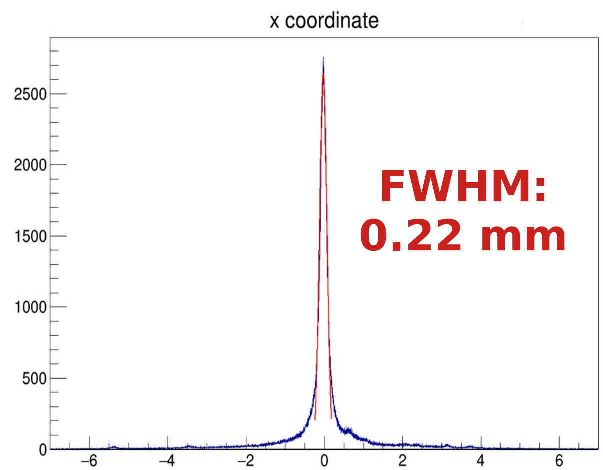

Same result for the y direction

2D Error distribution

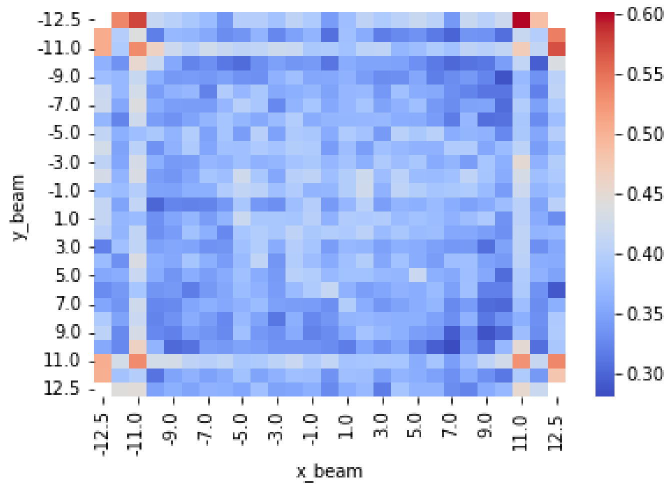

Difference real - predicted in the DOI direction

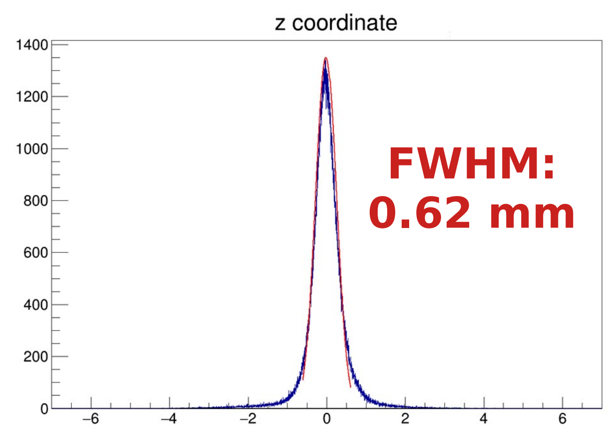

FOMs (mm)

	MAE	eucliden distance	FWHM
2D	-	0.27	0.22
3D	0.21	0.44	0.62

FOMs (mm)

	MAE	euclidean distance	FWHM
2D	-	0.27	0.22
3D	0.21	0.44	0.62

Analytical method

- FWHM and median 2D euclidean distance of 0.32 mm and 0.35 mm for x and y positions estimation, respectively.
- 1.8 mm for the spatial resolution in the case of the DOI estimation.

Outline

- Introduction to Compton Cameras
- MACACO Compton Camera
- **Application of Neural Networks to Enhance MACACO Compton Camera Imaging**
  - Event Selection with Multi-Energy Radioactive Sources
  - Photon Interaction Localization in Monolithic Crystals
  - **Background Reduction for Proton Range Verification**
- Conclusions

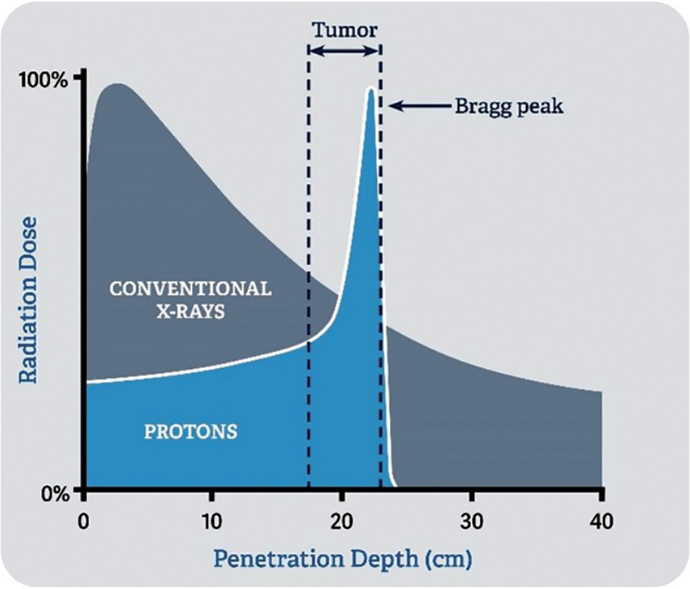
Tumor
100%
Bragg peak
Radiation Dose
CONVENTIONAL
X-RAYS
PROTONS
0%
0
10
20
30
40
Penetration Depth (cm)

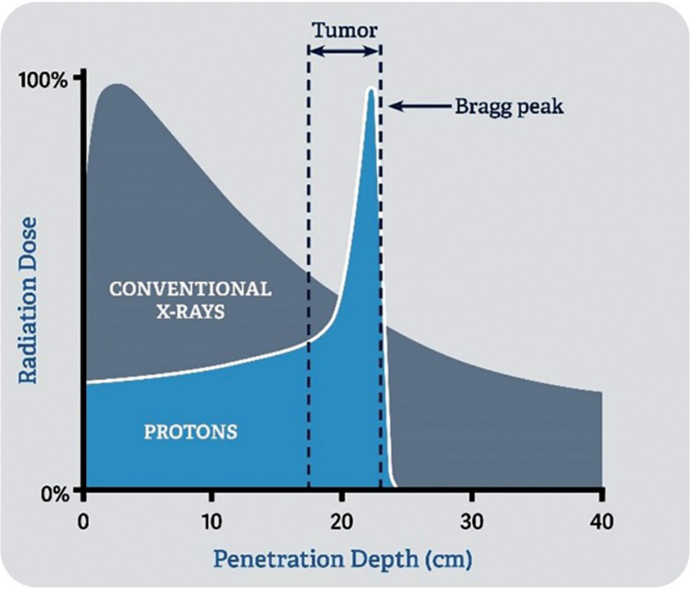
Tumor
Bragg peak
100%
0%
Radiation Dose
CONVENTIONAL
X-RAYS
PROTONS
0
10
20
30
40
Penetration Depth (cm)

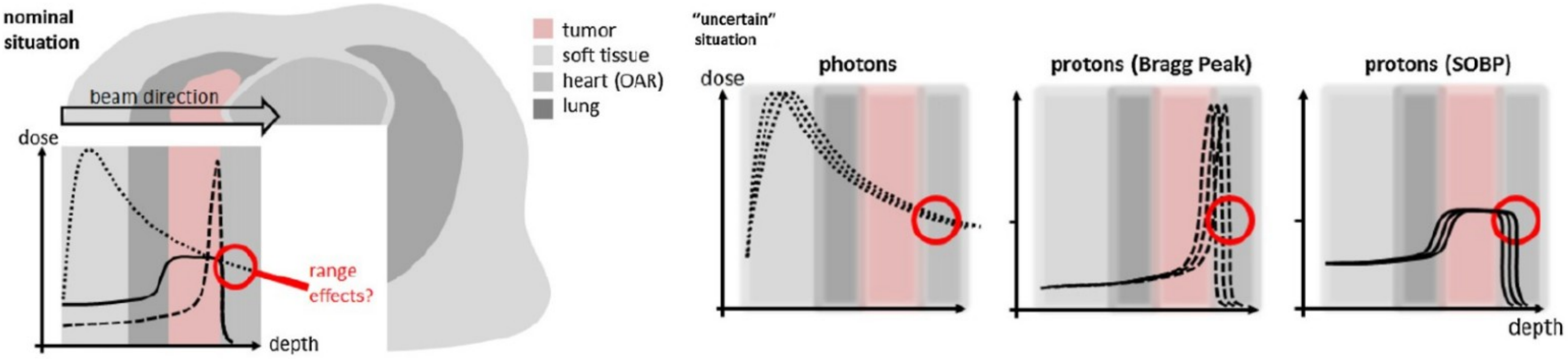
nominal
situation
beam direction
dose
depth
range
effects?
tumor
soft tissue
heart (OAR)
lung
"uncertain"
situation
dose
photons
protons (Bragg Peak)
protons (SOBP)
depth

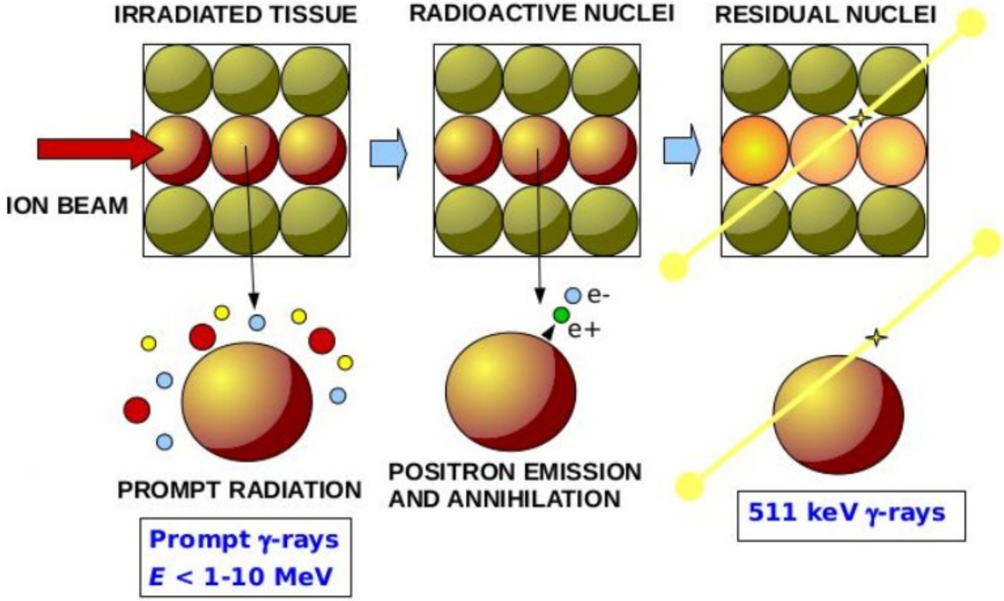
IRRADIATED TISSUE
RADIOACTIVE NUCLEI
RESIDUAL NUCLEI
ION BEAM
e-
e+
PROMPT RADIATION
POSITRON EMISSION AND ANNIHILATION
Prompt γ-rays
E < 1-10 MeV
511 keV γ-rays

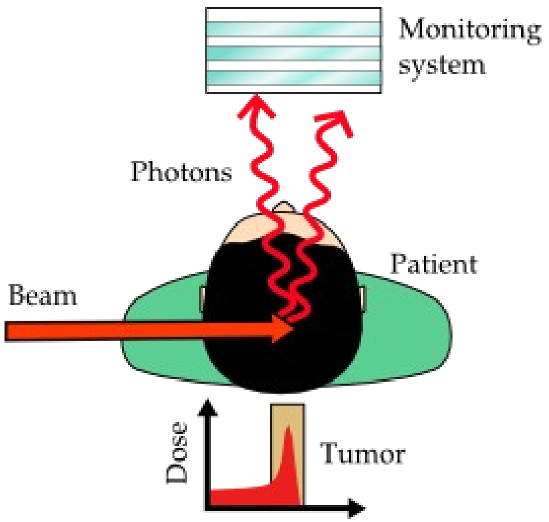
Monitoring system
Photons
Patient
Beam
Dose
Tumor

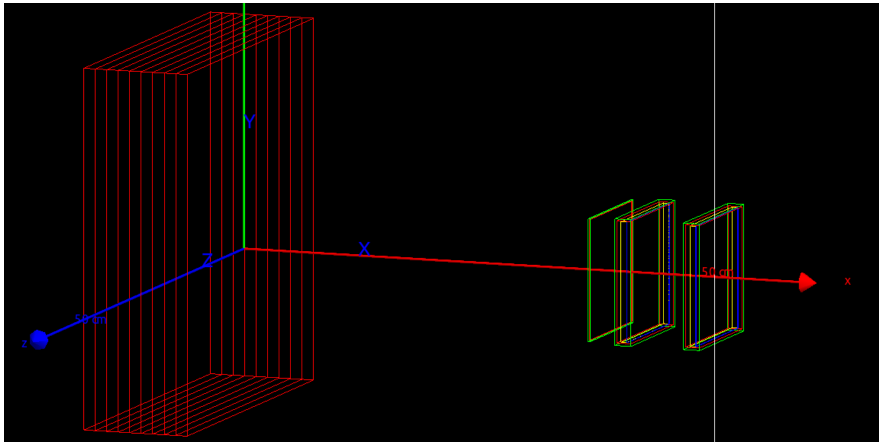

MACACO III simulation in Gate v8.2

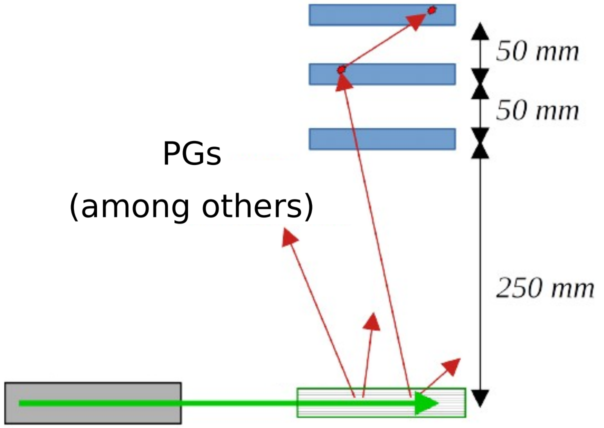

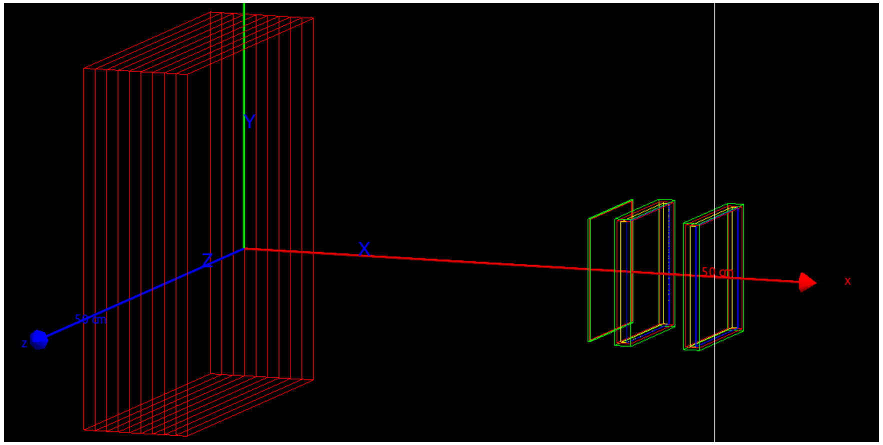

MACACO III simulation in Gate v8.2

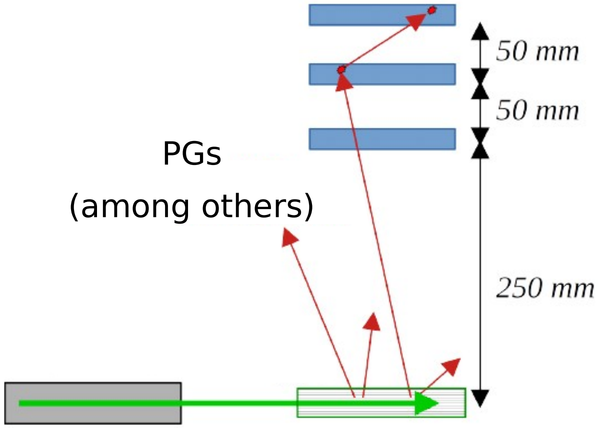

Data	Type
Signal true	0
background	1

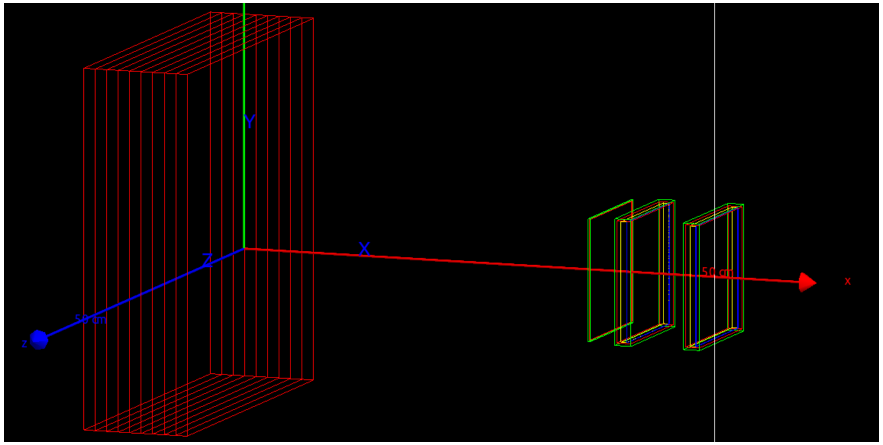

MACACO III simulation in Gate v8.2

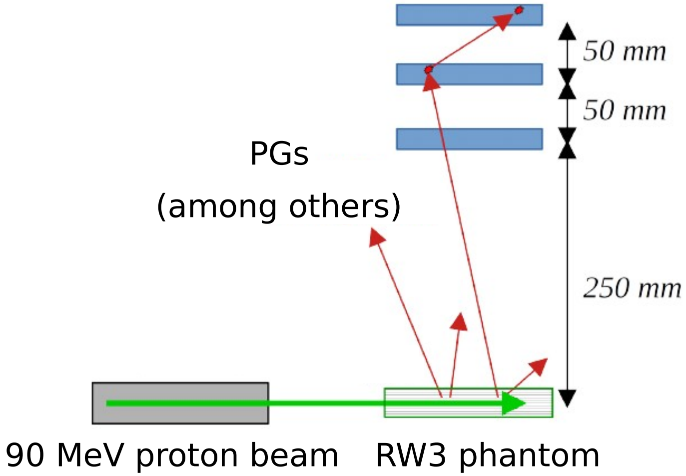

Data	**Type**
Signal true	0
background	1

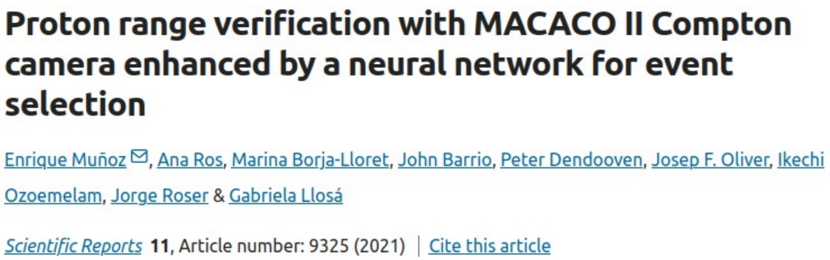

Proton range verification with MACACO II Compton camera enhanced by a neural network for event selection

Enrique Muñoz, Ana Ros, Marina Borja-Lloret, John Barrio, Peter Dendooven, Josep F. Oliver, Ikechi Ozoemelam, Jorge Roser & Gabriela Llosá

Scientific Reports **11**, Article number: 9325 (2021) | Cite this article

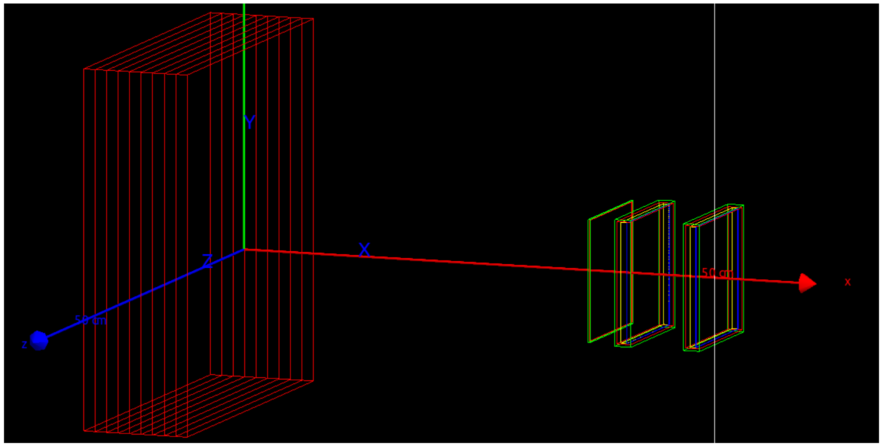

MACACO III simulation in Gate v8.2

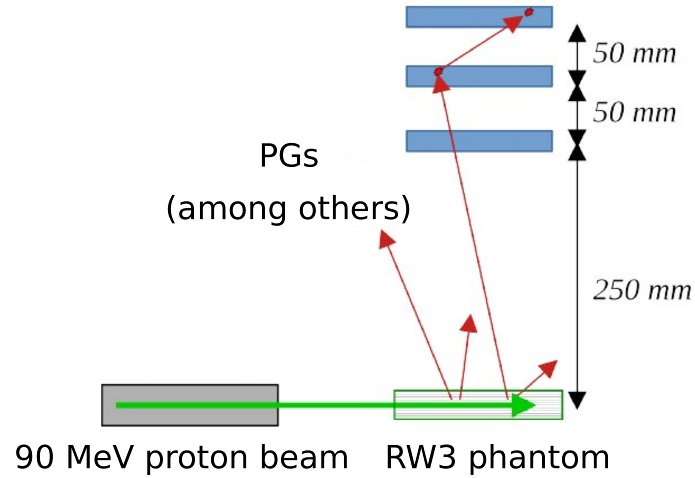

Data	Type
Signal true	0
background	1

Proton range verification with MACACO II Compton camera enhanced by a neural network for event selection

Enrique Muñoz, Ana Ros, Marina Borja-Lloret, John Barrio, Peter Dendooven, Josep F. Oliver, Ikechi Ozoemelam, Jorge Roser & Gabriela Llosá

Scientific Reports **11**, Article number: 9325 (2021) | Cite this article

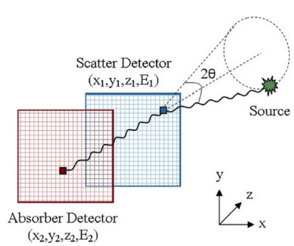

+

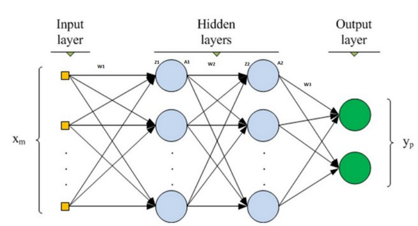

=

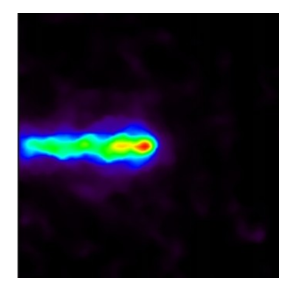

NNs trainning

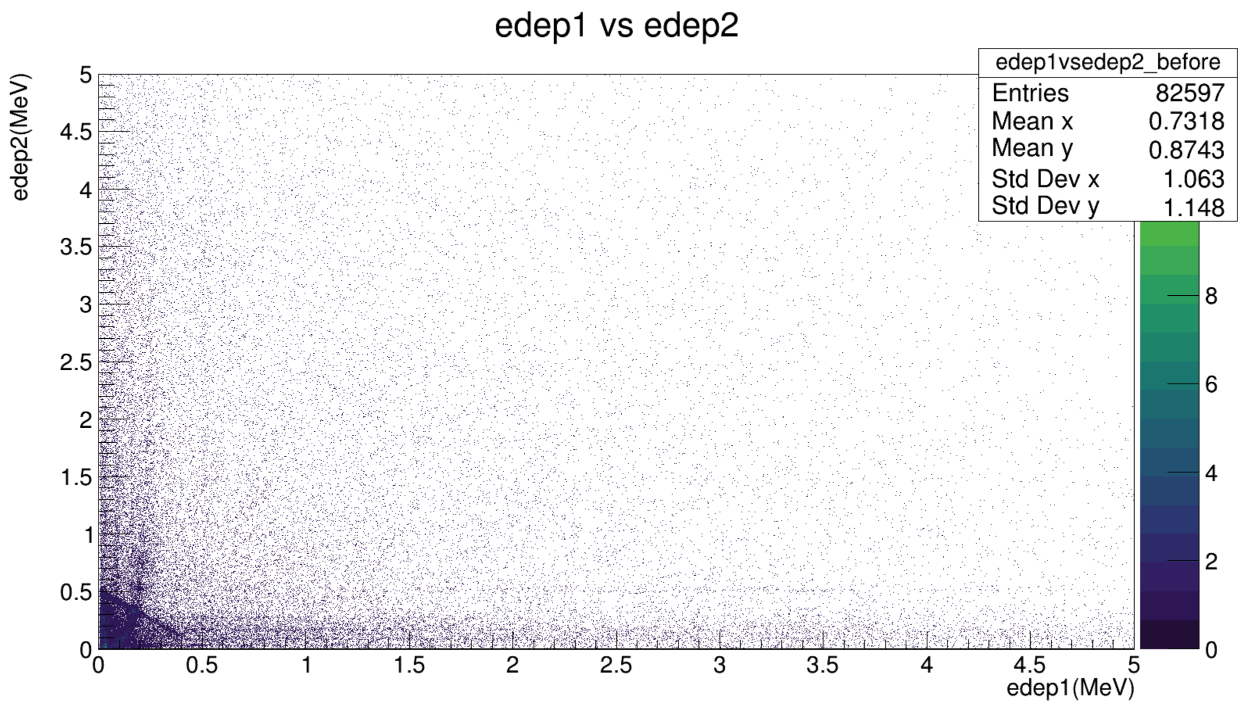

Deposited energy in the first plane
vs
Deposited energy in the second plane

	NN
Layers (# of neurons)	1-1-1 (80-40-1)
Optimizer	Adam
Learning rate	0.005
Activation	ReLU sigmoid
Batch size	500
Epoch	50

Experimental setup

- CCB in Krakow

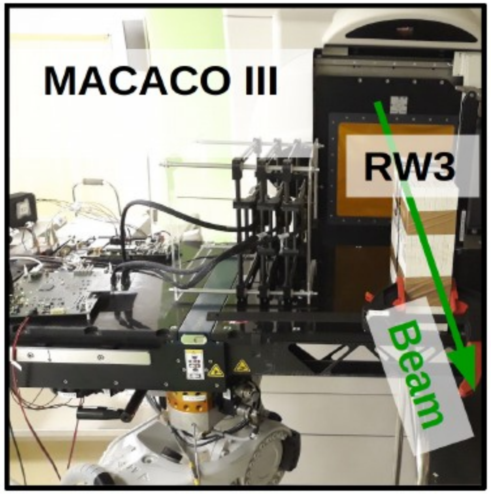

- 90 MeV protons impinging on RW3 phantom

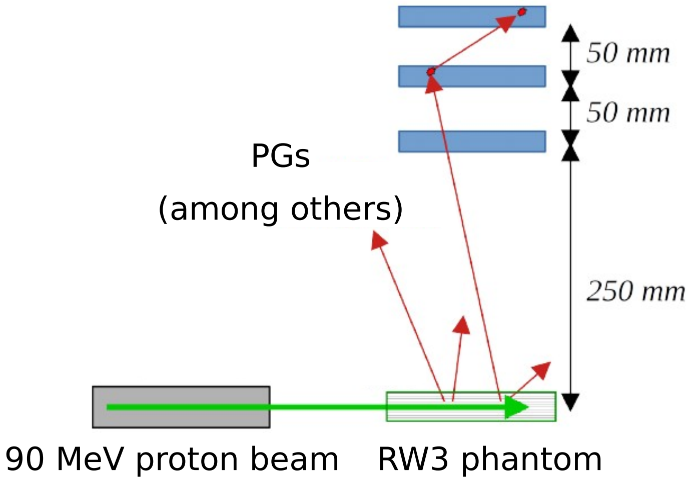

Experimental setup

- CCB in Krakow

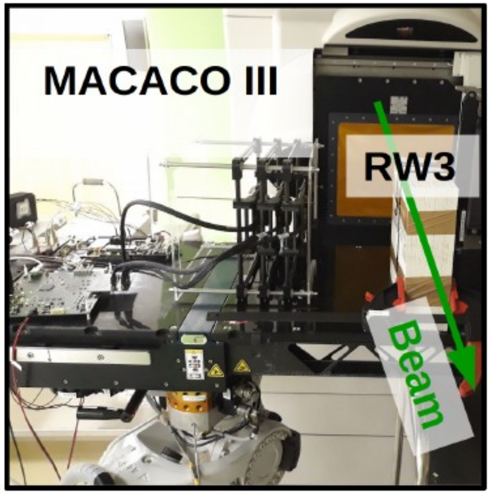

- 90 MeV protons impinging on RW3 phantom

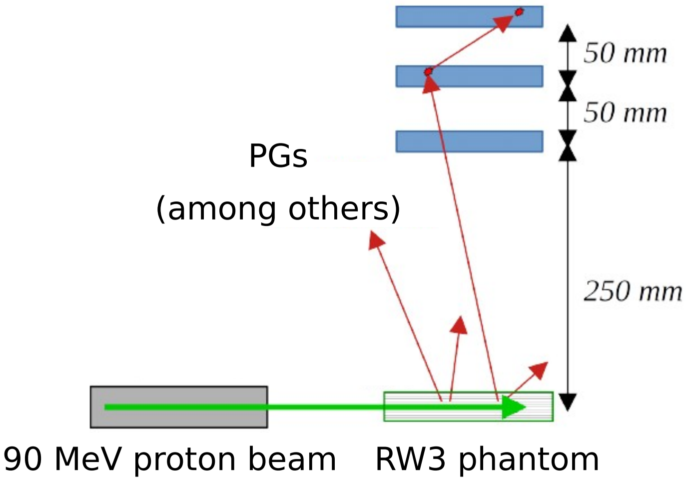

- 2 mm displacements changing proton energy to 88.38 and 91.62 MeV

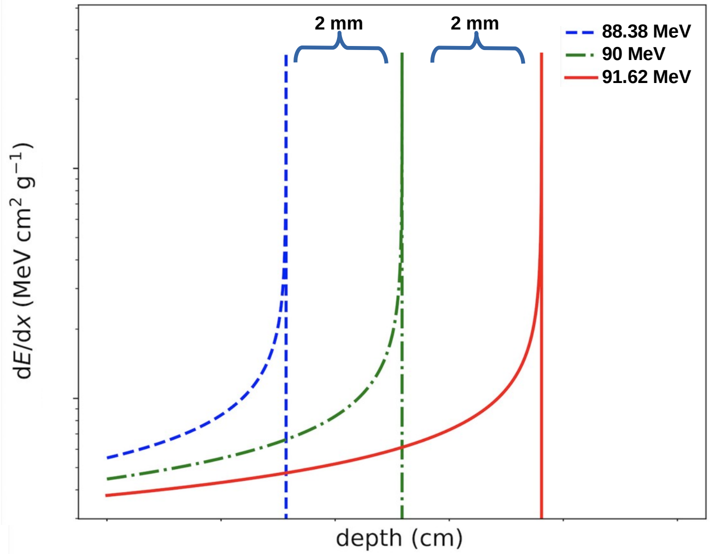

90 MeV

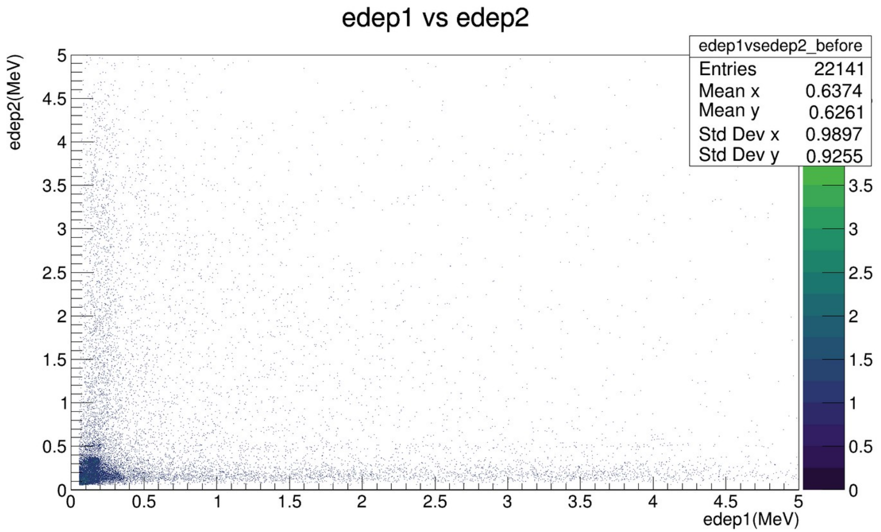

Deposited energy in the first plane
vs
Deposited energy in the second plane

NN selected data

90 MeV

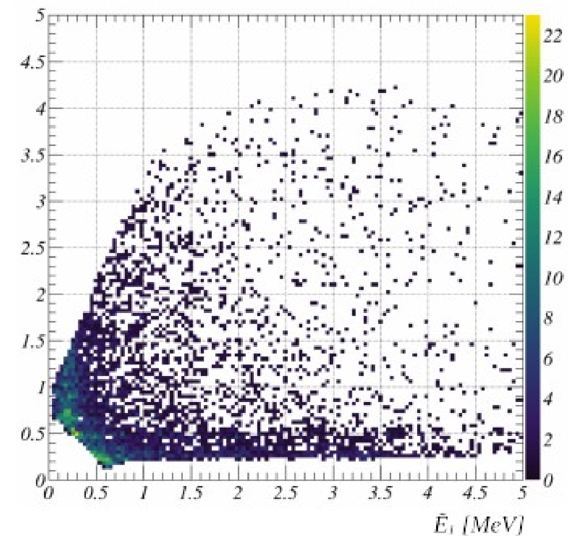

90 MeV

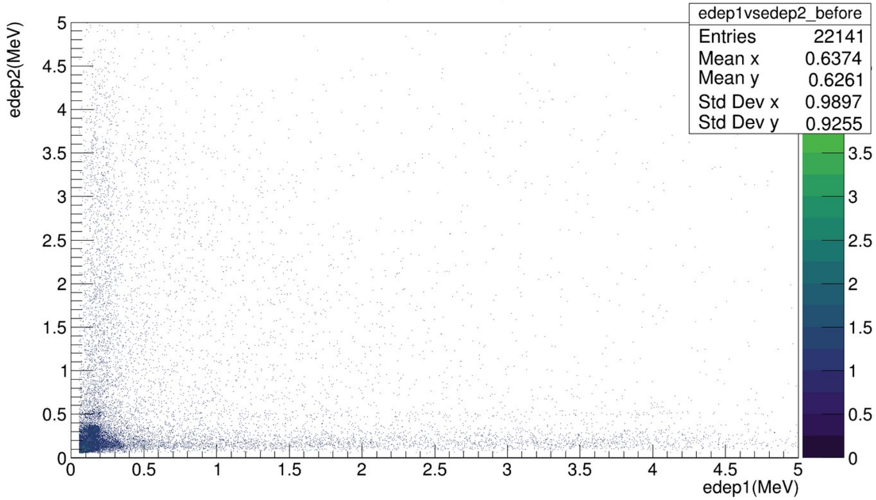

Deposited energy in the first plane
vs
Deposited energy in the second plane

NN selected data

90 MeV

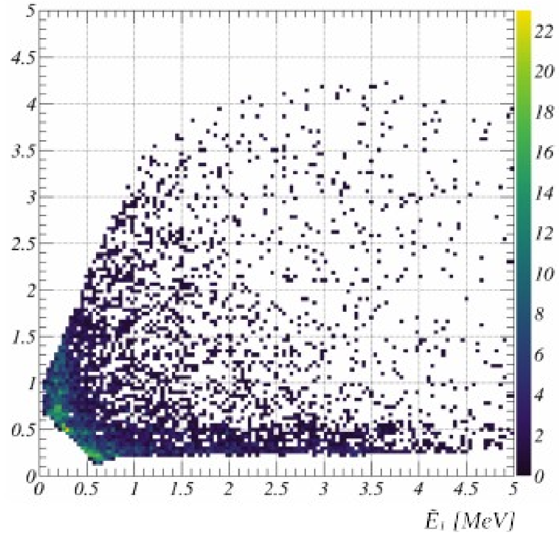

88.38 MeV

90 MeV

91.62 MeV

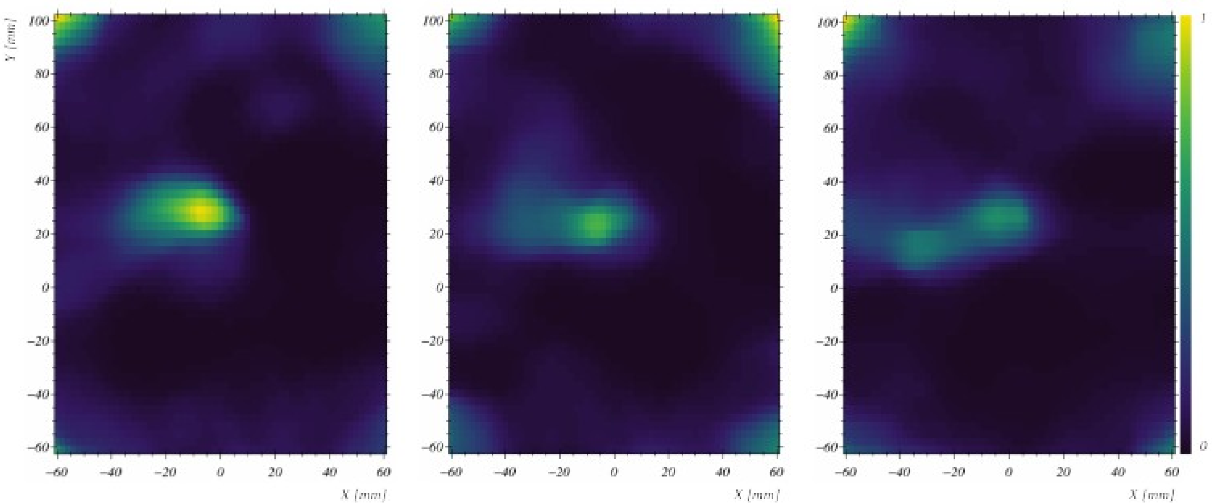

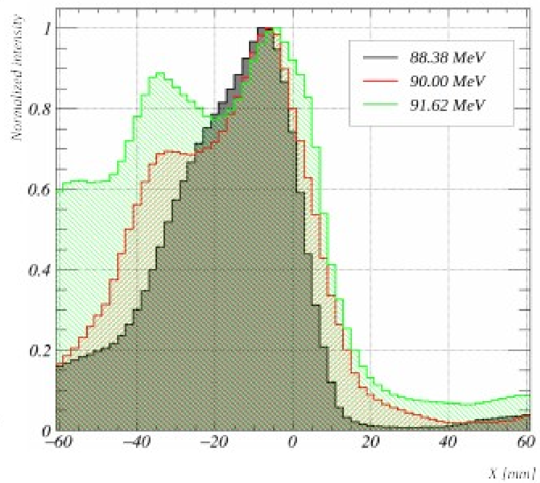

Profiles of the images with true signal data classified by the NN model.

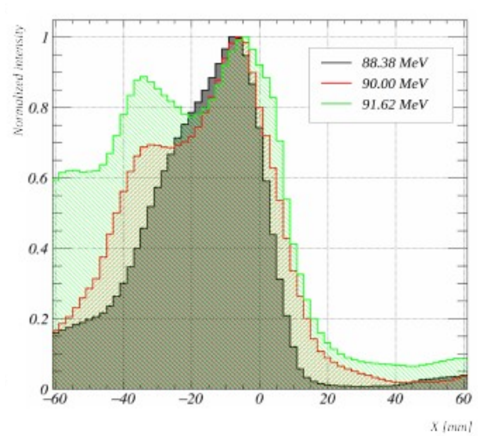

	Obtained displacements ±1.4 mm		
	88.38 – 90.00 MeV	90.00 – 91.62 MeV	88.38 – 91.62 MeV
Maximum	2.0	2.0	4.0
R80	0.9	4.4	5.5
R50	3.5	2.0	5.5

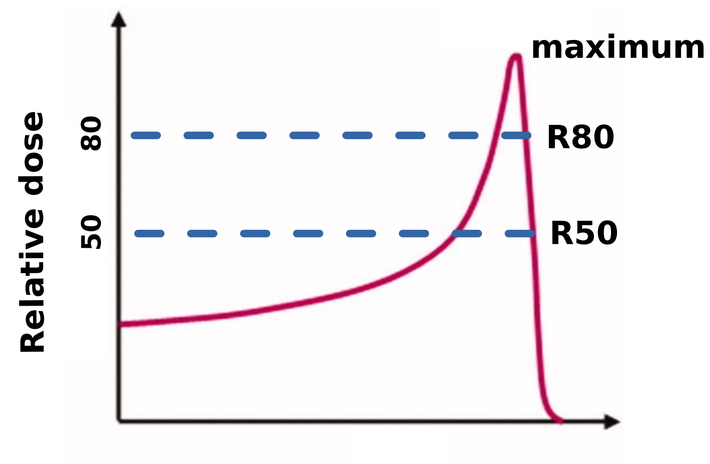

Profiles of the images with true signal data classified by the NN model.

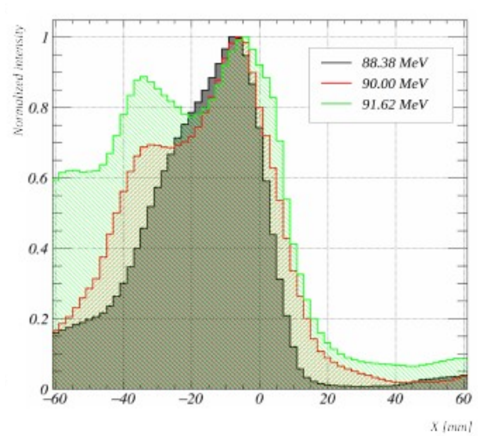

	Obtained displacements ±1.4 mm		
	88.38 – 90.00 MeV	90.00 – 91.62 MeV	88.38 – 91.62 MeV
Maximum	2.0	2.0	4.0
R80	0.9	4.4	5.5
R50	3.5	2.0	5.5

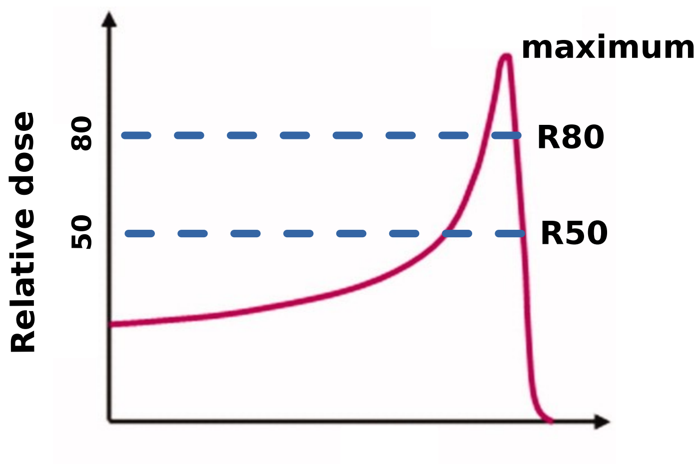

Profiles of the images with all experimental events applying energy cuts prior to reconstruction.

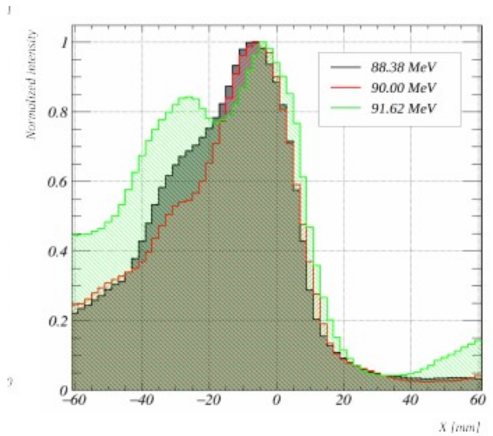

	Obtained displacements ±1.4 mm		
	88.38 – 90.00 MeV	90.00 – 91.62 MeV	88.38 – 91.62 MeV
Maximum	2.0	0.0	2.0
R80	−0.3	3.1	3.4
R50	0.6	2.0	2.6

Ongoing work

Outline

- Introduction to Compton Cameras
- MACACO Compton Camera
- Application of Neural Networks to Enhance MACACO Compton Camera Imaging
  - Event Selection with Multi-Energy Radioactive Sources
  - Photon Interaction Localization in Monolithic Crystals
  - Background Reduction for Proton Range Verification
- **Conclusions**

Conclusions

- We have successfully applied neural networks to enhance the performance of Compton cameras in various imaging tasks.
- Neural networks were used in three distinct scenarios: event selection, photon interaction localization, and background reduction, demonstrating positive results in each case.
- The results showed promising improvements, indicating that neural networks have the potential to significantly enhance the detector performance.
- As newcomers to the field of neural networks, we recognize that there is still room for improvement and further refinement of our models.

Acknowledgments

- This work has received funding from the Spanish Ministerio de Ciencia e Innovación (PID2019-110657RB-I00, PID2022-143246OB-I00).

- Group members are supported by GVA Excellence programmes, UVEG Atracció de Talent, SEJIGENT and GVA Grisolía.

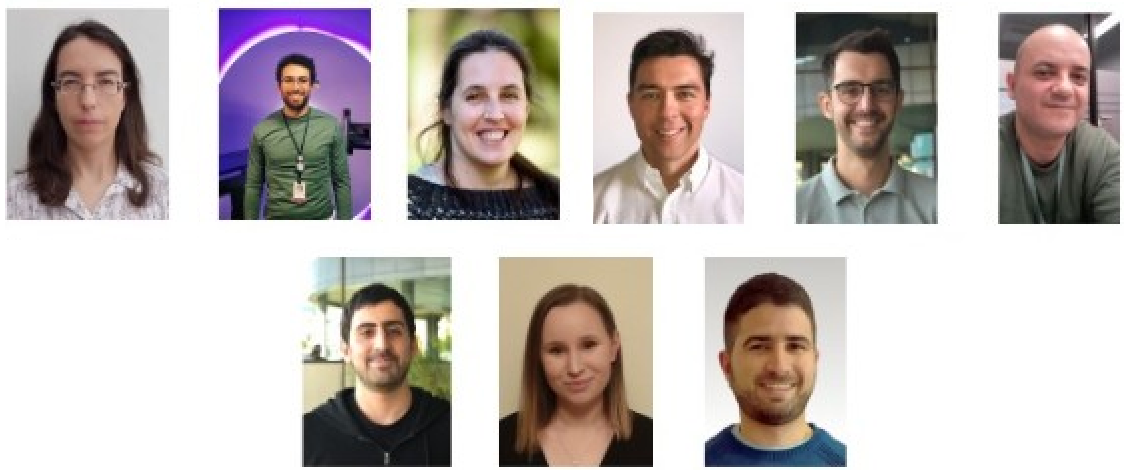

IFIC INSTITUT DE FÍSICA CORPUSCULAR · CSIC · VNIVERSITAT DE VALÈNCIA · IRIS · GOBIERNO DE ESPAÑA · MINISTERIO DE CIENCIA E INNOVACIÓN · AGENCIA ESTATAL DE INVESTIGACIÓN

http://ific.uv.es/iris


GRACIAS
a todos
¡hasta la proxima, te tendre en mente! Hannah

Enhancing Compton Camera Imaging with Neural Networks

J. Pérez-Curbelo, J. Roser, L. Barrientos, R. Viegas, M. Borja-Lloret,

J. V. Casaña, F. Hueso-González, A. Ros, K. Brzezinski, V. Sanz and G. Llosá

Instituto de Física Corpuscular IFIC (CSIC-UV)

http://ific.uv.es/iris

Image **R**econstruction, **I**nstrumentation and **S**imulations in medical applications

Table 6
Statistical results for events selection on simulated circular array data. Highlighted rows correspond to the selected cases for image reconstruction.

Model	Type 0	Background	TSP (%)	Recall
NNc	**136 282**	**41 600**	**77**	**83**
NNc_soft(0.3)	**143 648**	**54 164**	**73**	**87**
NNc_soft(0.4)	139 765	46 466	75	85
NNc_hard(0.6)	**123 363**	**29 139**	**81**	**75**
Cut in 600 keV	109 795	57 573	66	67

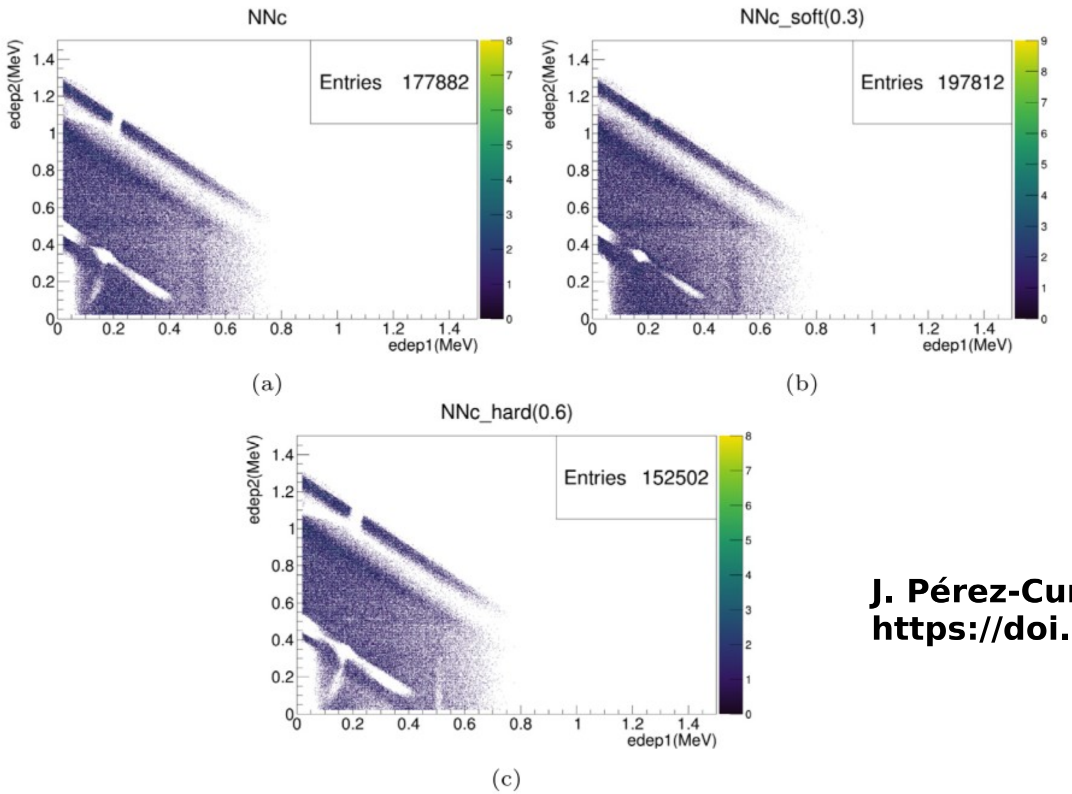

Fig. 7. Deposited energy in plane 2 vs. plane 1 of the CC for the selected events from the simulated circular array.

J. Pérez-Curbelo et al., Rad. Phys. and Chem (2024), https://doi.org/10.1016/j.radphyschem.2024.112166.

Thresholds study

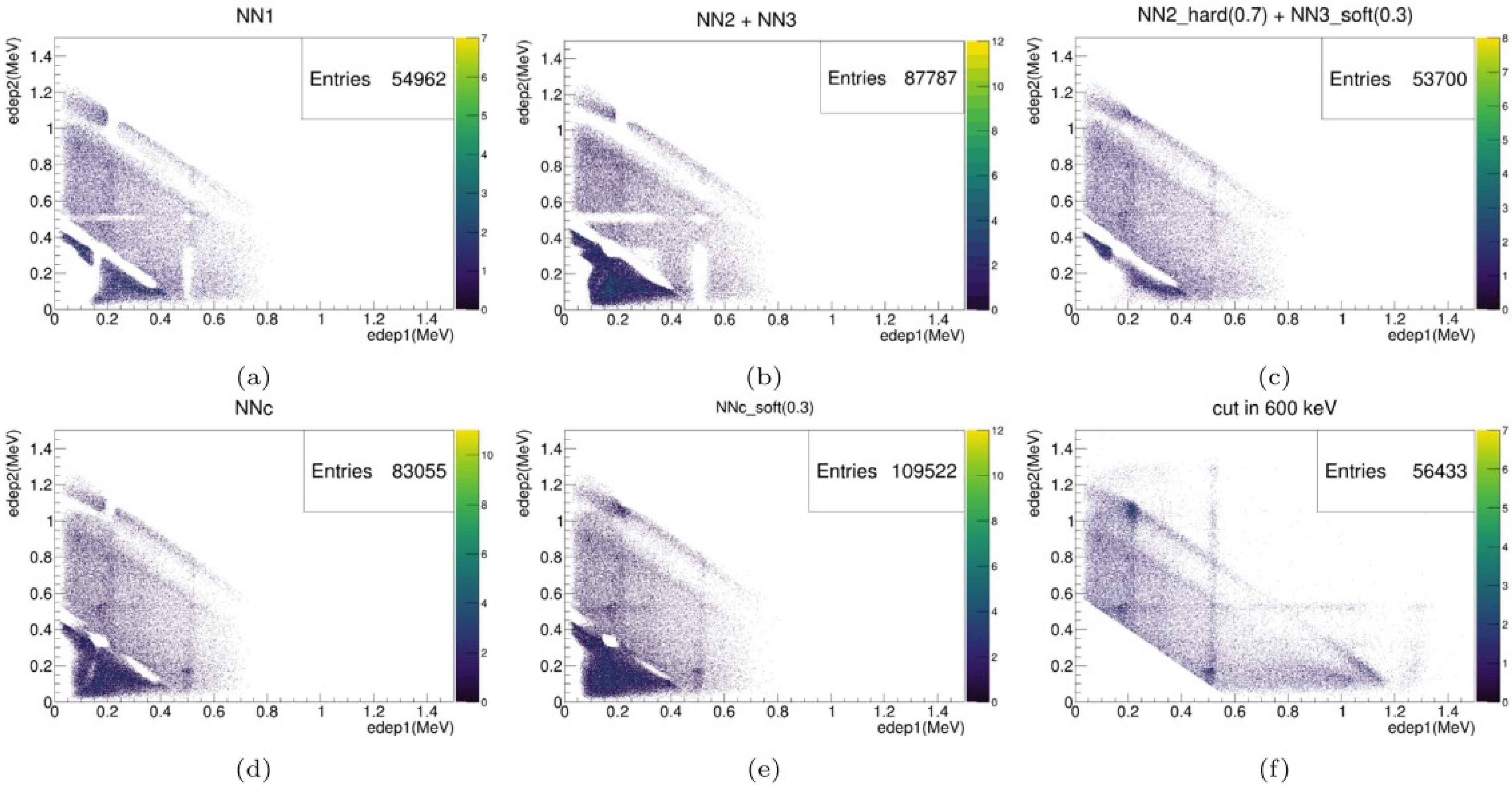

Fig. 10. Deposited energy in plane 2 vs. plane 1 of the CC for the selected events from the experimental circular array: (a,b,c,d,e) the NN models and (f) the energetic cut method.

J. Pérez-Curbelo et al., Rad. Phys. and Chem (2024), https://doi.org/10.1016/j.radphyschem.2024.112166.

Backup slides

Background reduction on simulated data

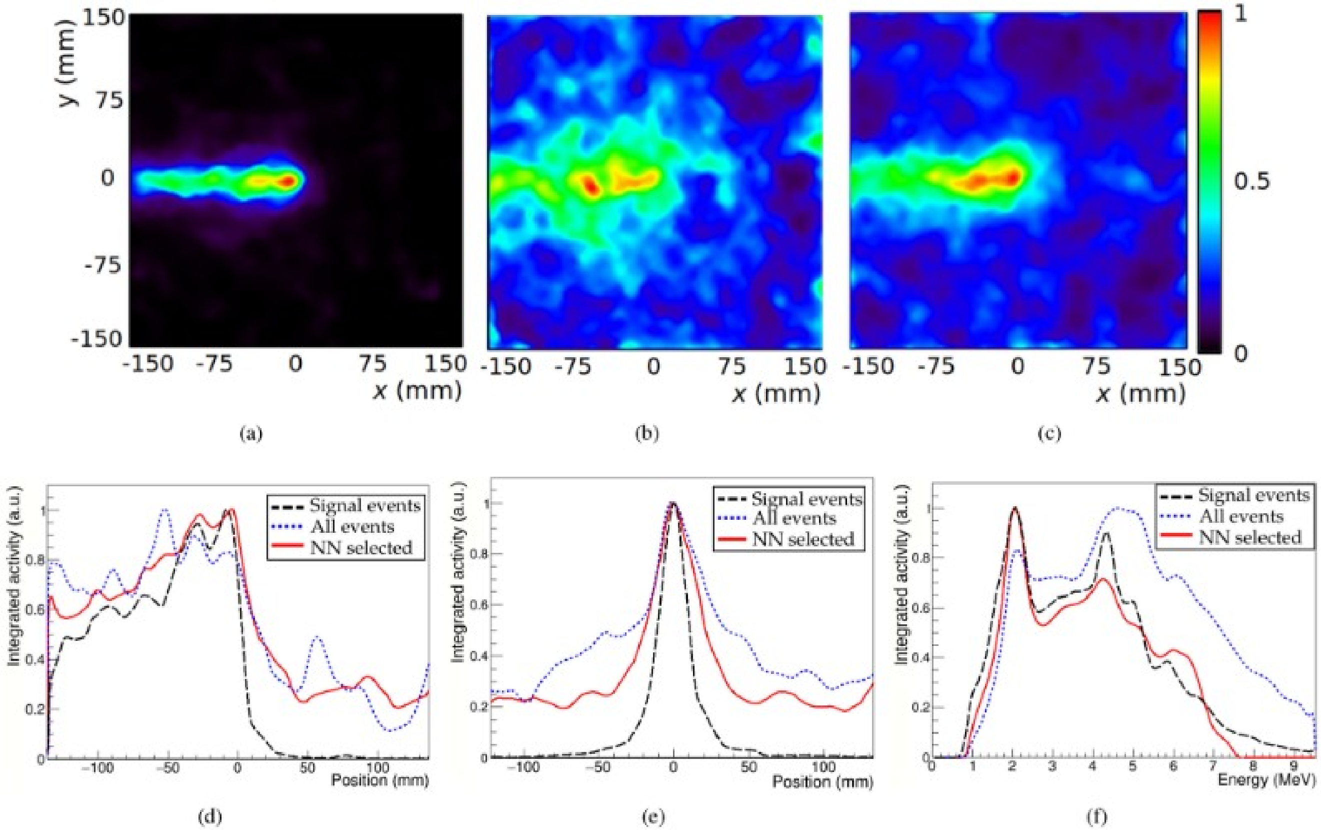

Figure 1. Reconstructed images at 4.4 MeV using three different simulated data sets: only true signal events (**a**), all events (**b**) and events selected by the trained NN (**c**). (**d**) Line profiles along the beam direction from the above images. (**e**) Transverse line profiles at the maximum position. (**f**) Energy spectra recovered after integration over the reconstructed image spatial domain.

Muñoz, E., et al., Sci Rep 11, 9325 (2021). https://doi.org/10.1038/s41598-021-88812-5